

SAR Maritime Applications

Currents and Objects

Martin Gade
Uni Hamburg, Institut für Meereskunde



SAR Maritime Applications

Friday, 11 Sep, Morning:

1 - History & Basics

- Introduction
- Radar/SAR History
- Basics
- Scatterometer

2 - Wind and Waves

- SAR Wind Fields
- Storms, Tropical Cyclones
- Ocean Surface Waves
- Oceanic Internal Waves
- Marine Surface Films
- Rain

Friday, 11 Sep, Afternoon:

3 - Currents and Objects

- Surface Currents
- Sea Bottom Topography
- Ship Detection
- Oil Pollution Monitoring
- Sea Ice

4 - Exercises

- Sentinel 1 Toolbox:
- Calibration, Georeferencing,
- Wind Fields, Oil Pollution,
- Radar Contrast,
- Statistics

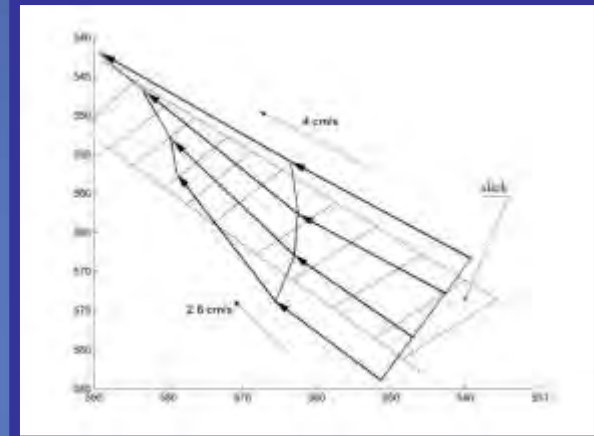


Surface Currents

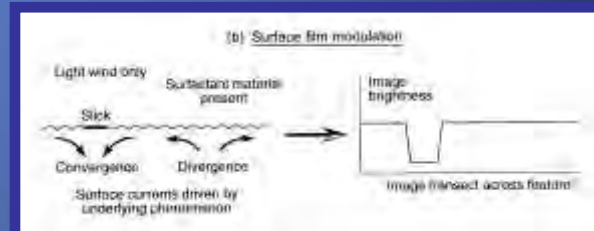
SAR Imaging of Surface Currents



Slicks & eddies



[Gade et al., 1998]

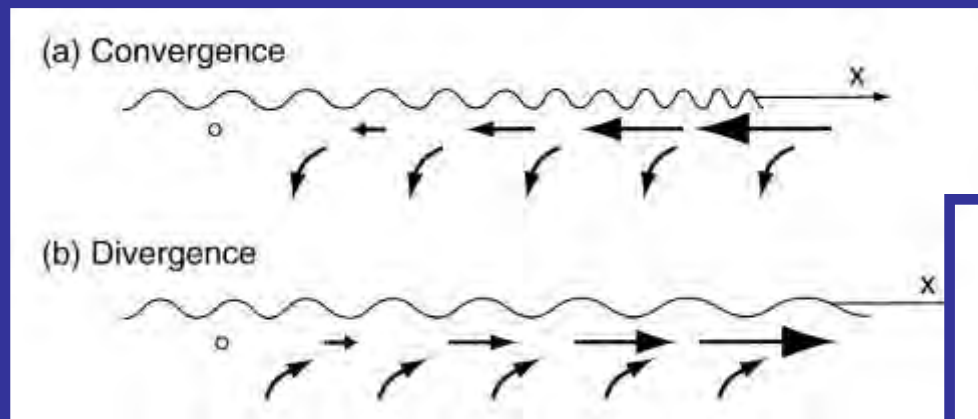


[Robinson, 2003]

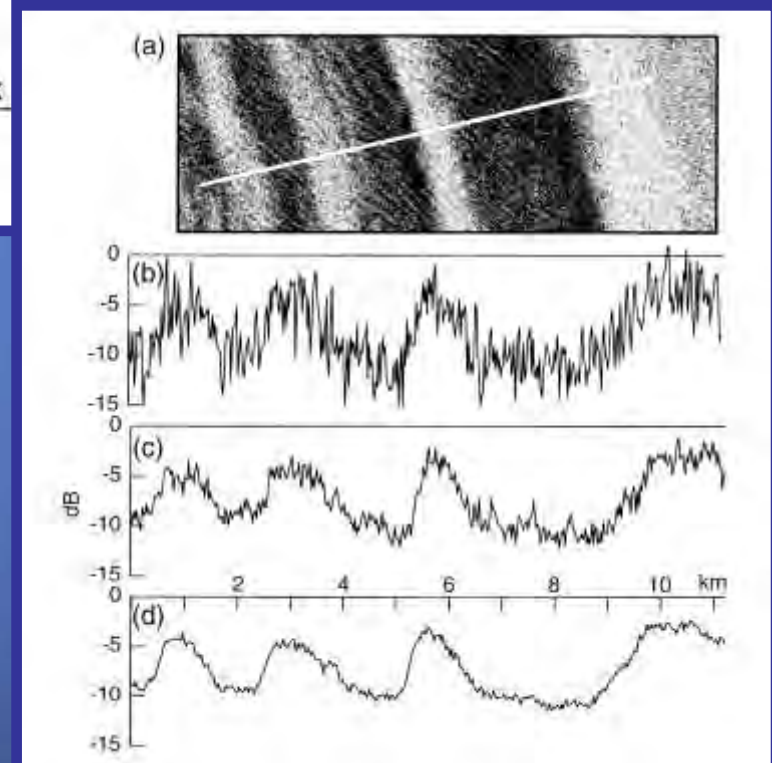
ERS SAR Image (C-VV; 70 km × 70 km)
Bering Strait
(24 June 1997, 22:30 UTC, © ESA)

Hydrodynamic Processes at the Sea Surface

Imaging by SAR

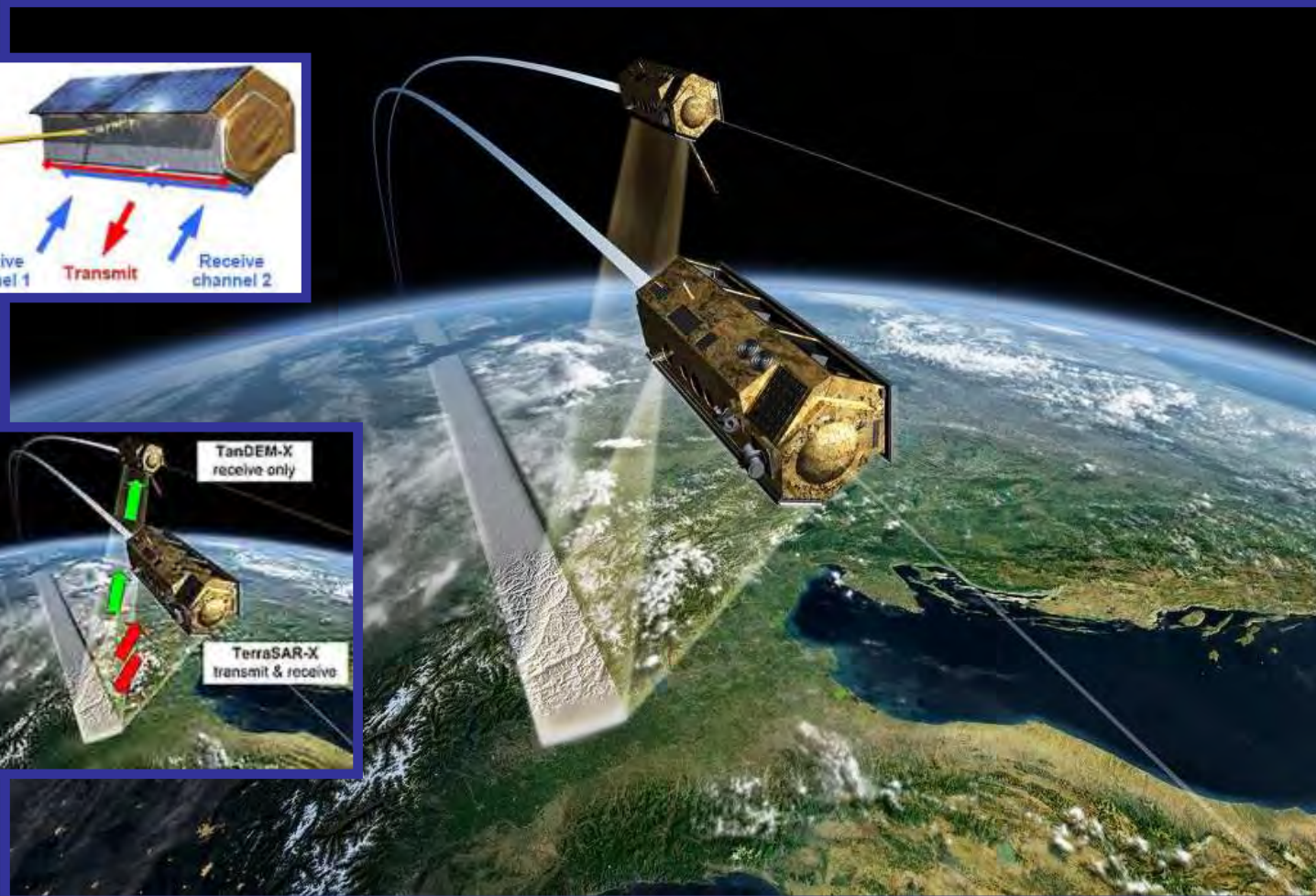
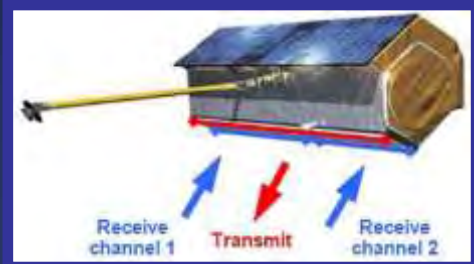


[Robinson, 2003]



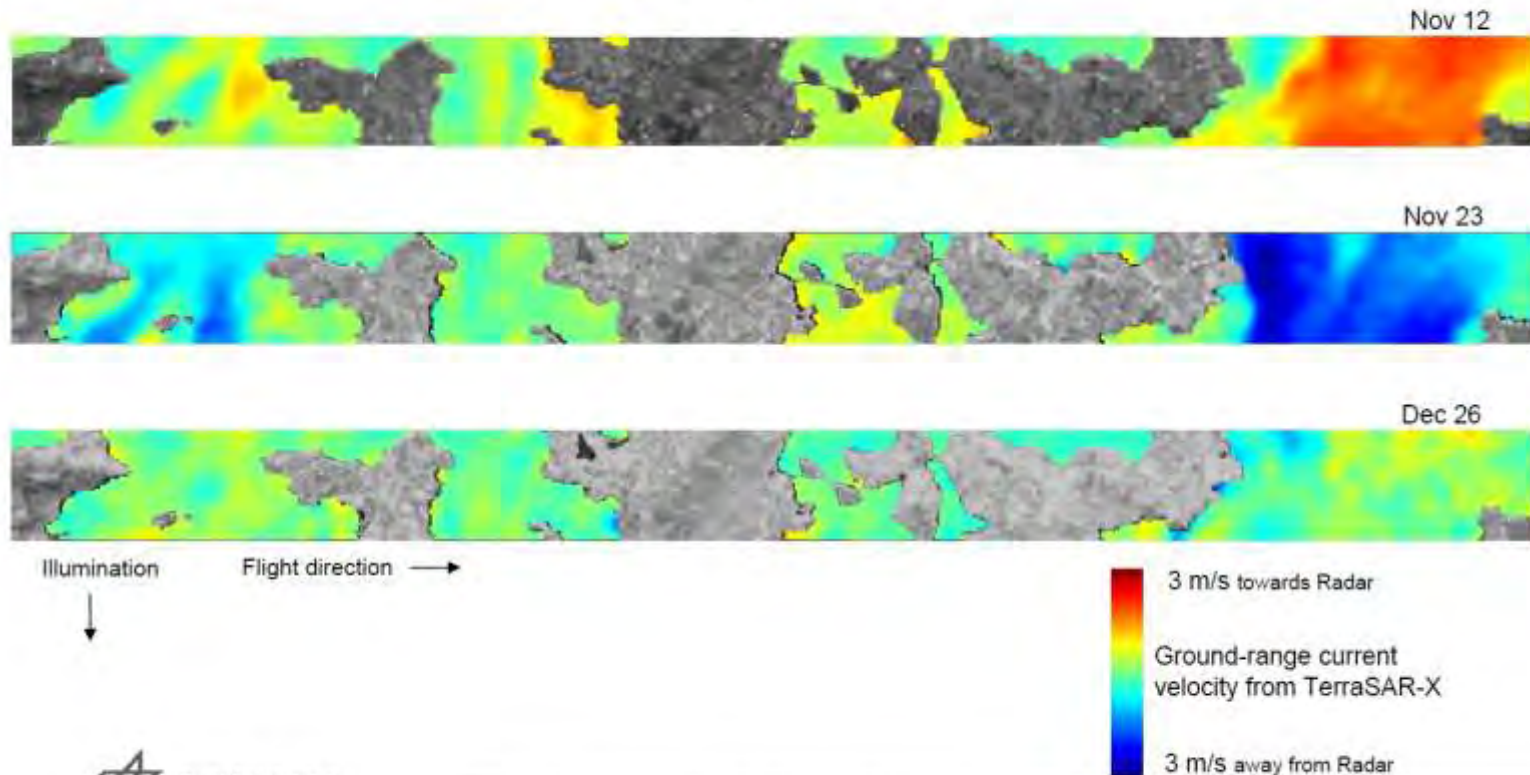
Along-Track Interferometric (ATI) SAR

TerraSAR-X / TanDEM-X



Along-Track Interferometric (ATI) SAR

Surface Current Velocities from TerraSAR-X ATI (AS-Mode) Orkney Islands, 2009

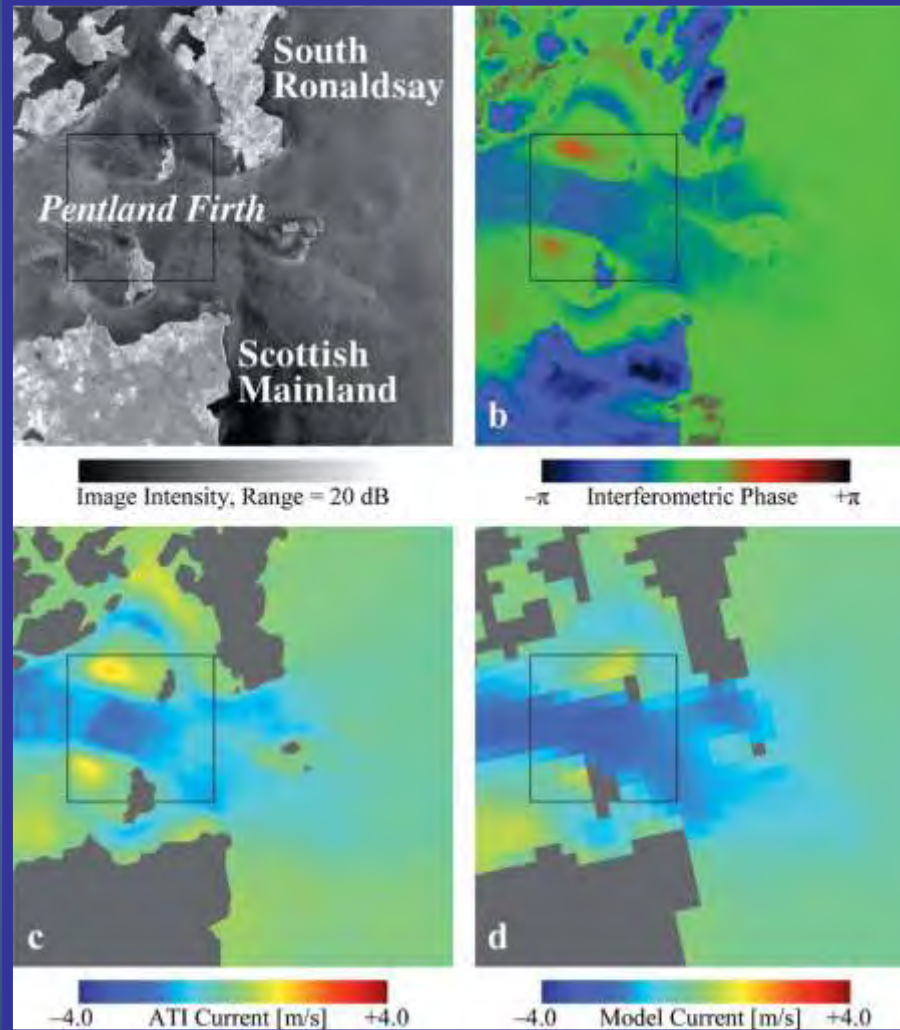


Deutsches Zentrum
für Luft- und Raumfahrt e.V.
in der Helmholtz-Gemeinschaft

Current estimation: R. Romeiser (University of Miami), Pre-Processing: S. Suchandt (DLR)

Along-Track Interferometric (ATI) SAR

TanDEM-X SAR Image
(X-VV; 30 km × 30 km)
Pentland Firth (Scotland)
(26 February 2012,
06:41 UTC, © DLR)



Interferometric
phase image

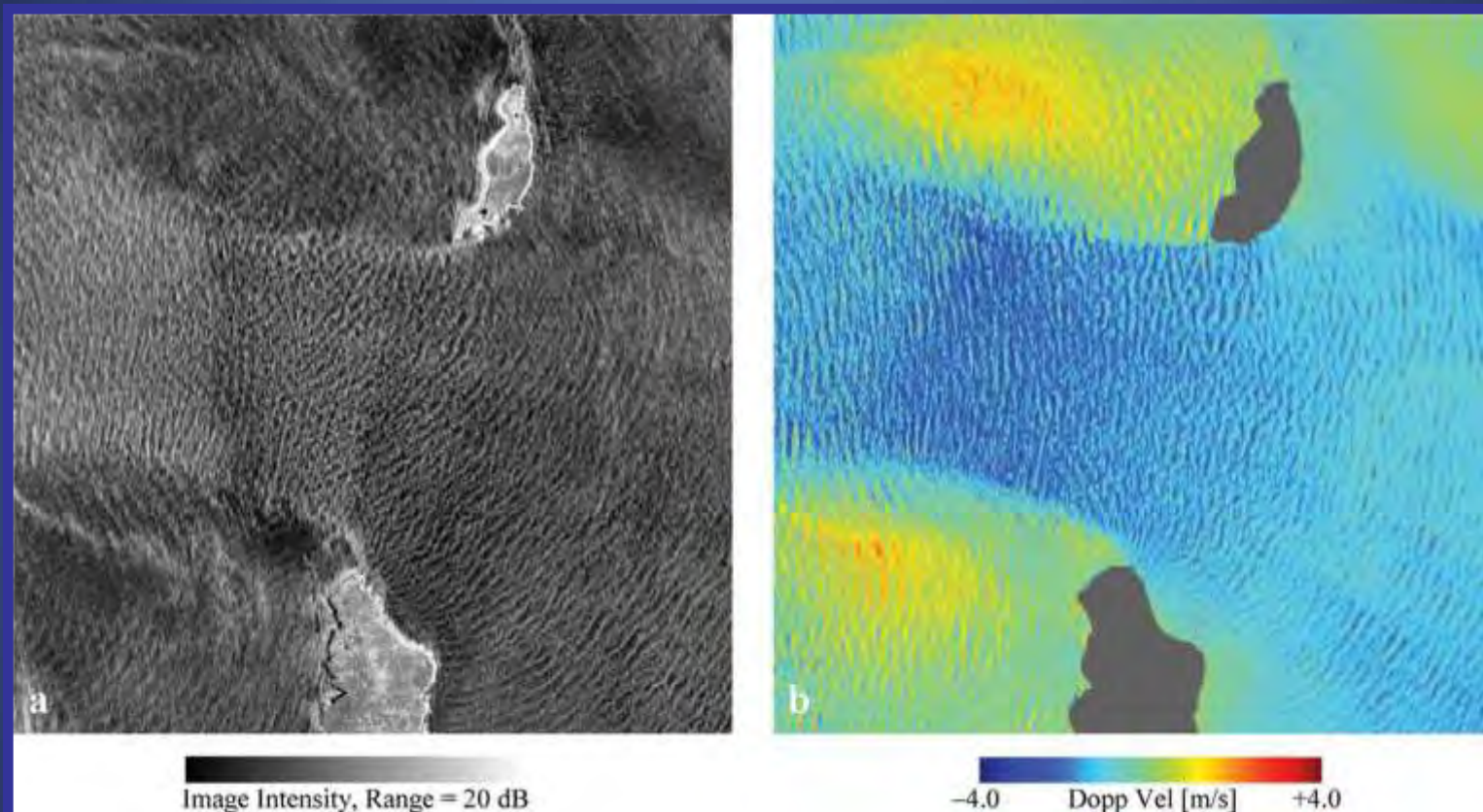
radar look direction

Derived line-of-sight
current field

Reference current field
from numerical tide
computation system

[Romeiser, 2013]

Along-Track Interferometric (ATI) SAR



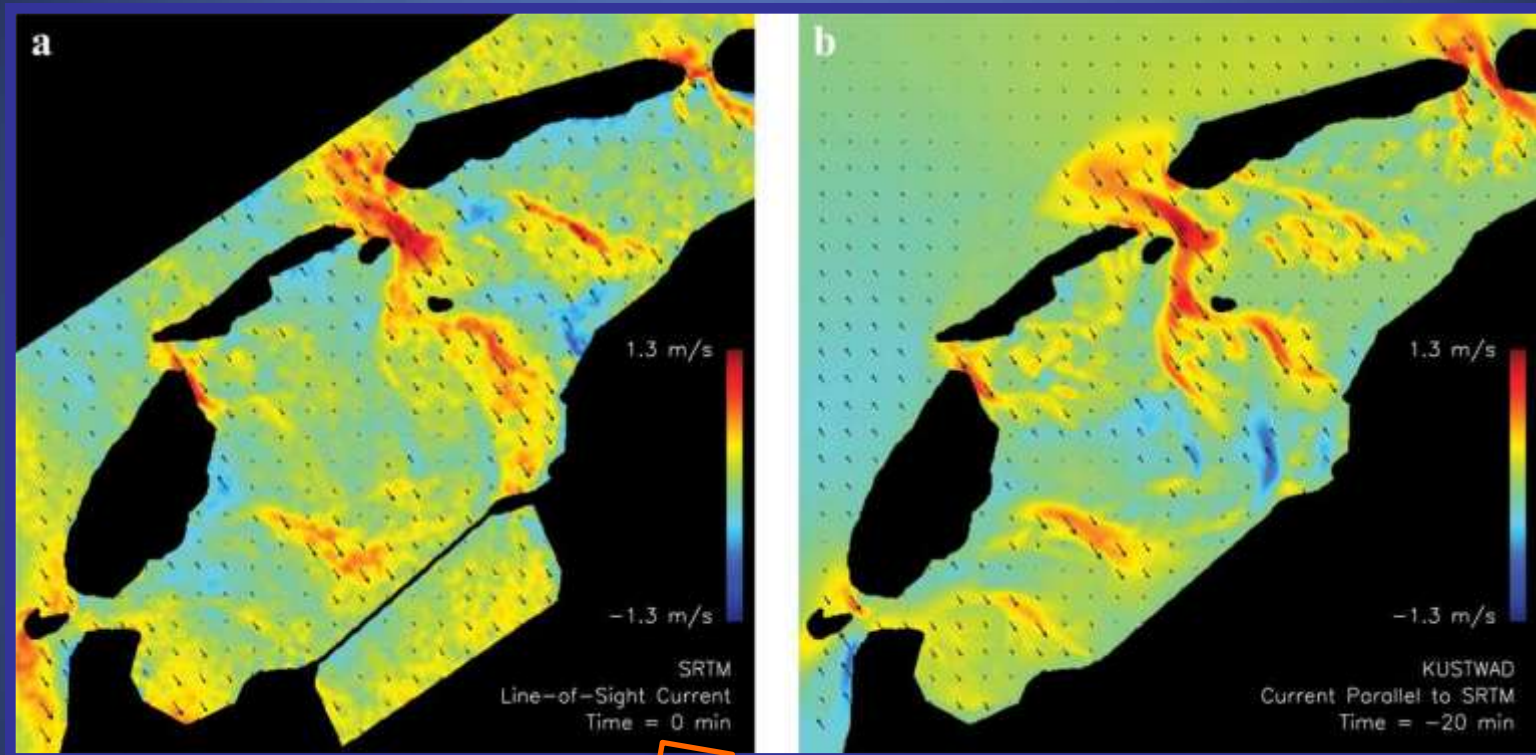
TanDEM-X SAR Image (X-VV; 10 km × 10 km)
Pentland Firth (Scotland)
(26 February 2012, 06:41 UTC, © DLR)

Derived line-of-sight current field:
full-resolution Doppler velocity image

radar look direction

[Romeiser, 2013]

Along-Track Interferometric (ATI) SAR



SRTM (X-VV; 70 km × 70 km)
Dutch Wadden Sea
(15 February 2000, 12:34 UTC)

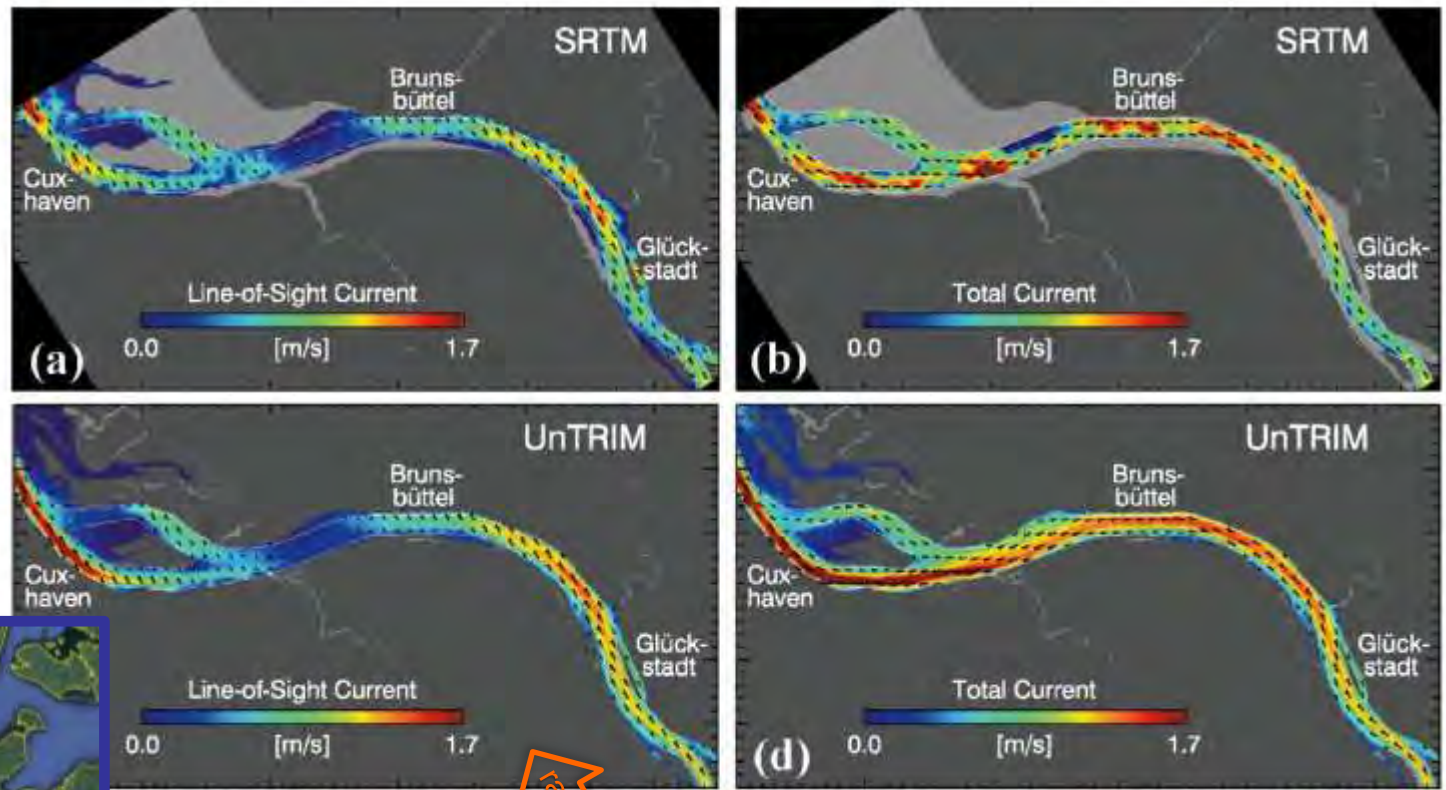
Reference current field from a
numerical circulation model

[Romeiser, 2013]

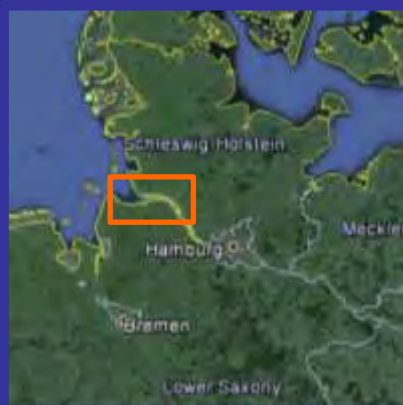
Along-Track Interferometric (ATI) SAR

SRTM (X-VV;
55 km × 30 km)
Elbe river

Current field
from a
numerical model

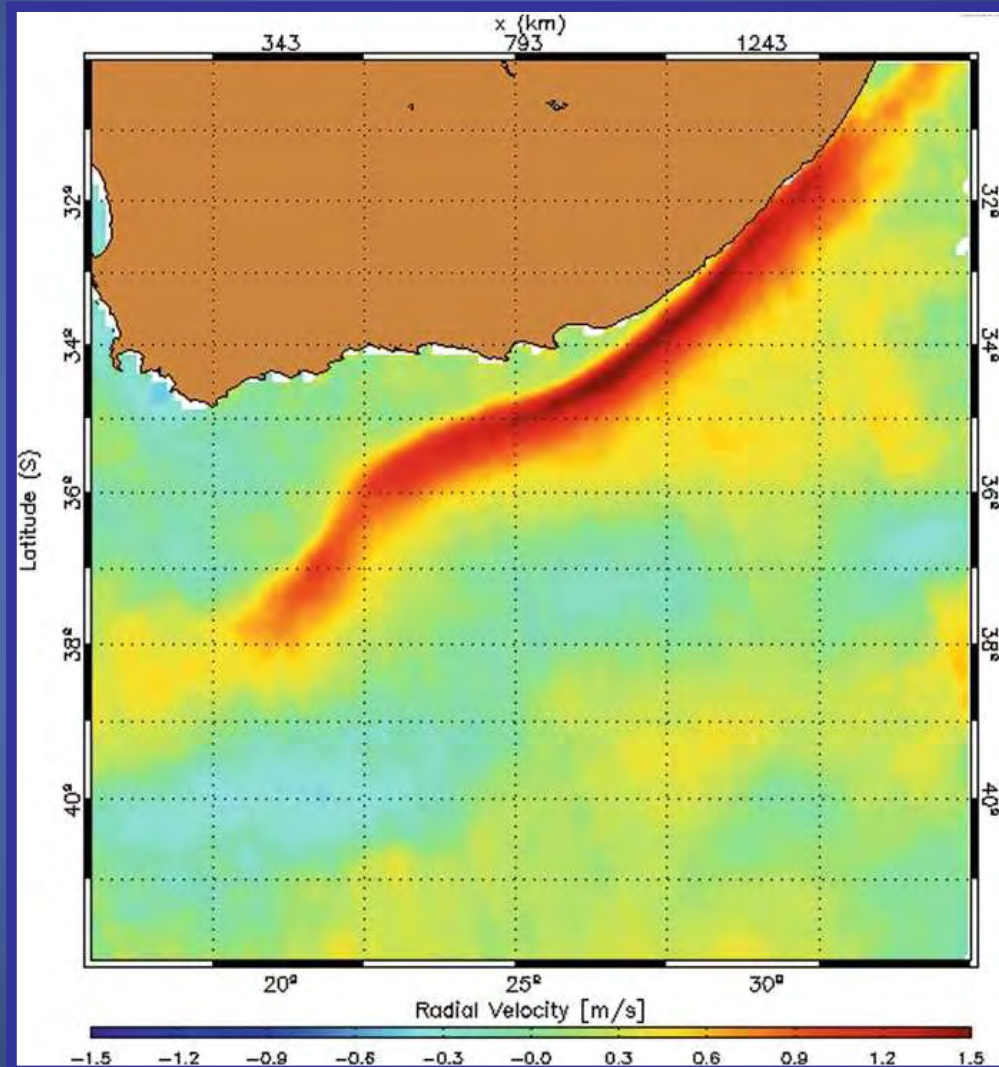


[Barale & Gade, 2008]



Radial Doppler Velocities from SAR Imagery

Mean radial Doppler velocities derived from 4 years ('07-'11) ASAR data



Mean westward current;
Agulhas Current (S Africa)

[Barale & Gade, 2014]



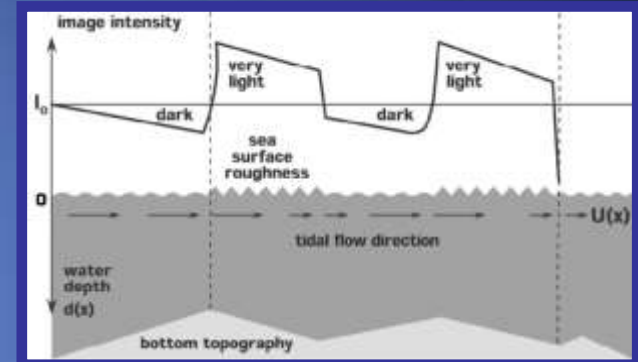
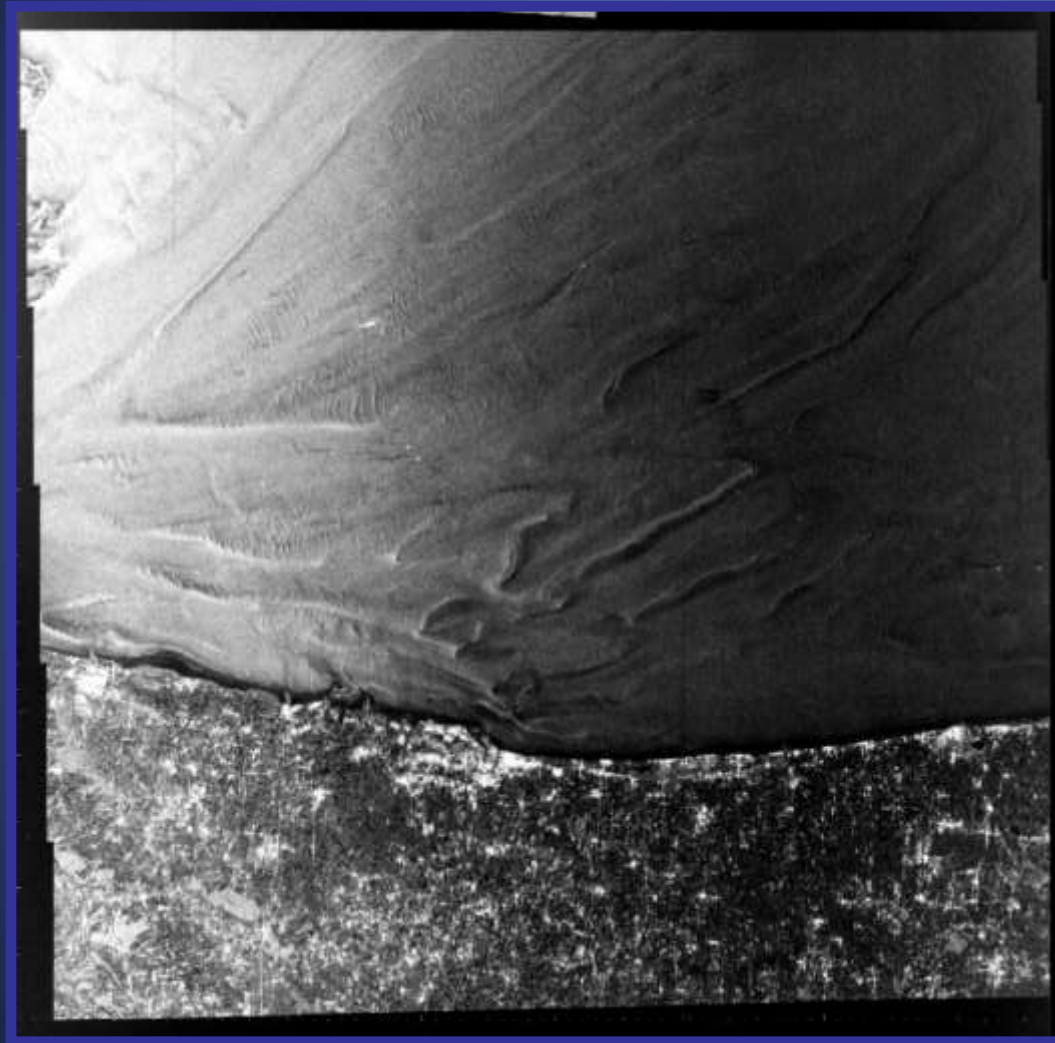
Surface Currents Take-Home Messages

Derivation of sea-surface currents:
tracking of features
Along-Track Interferometry
Doppler velocities



Sea Bottom Topography

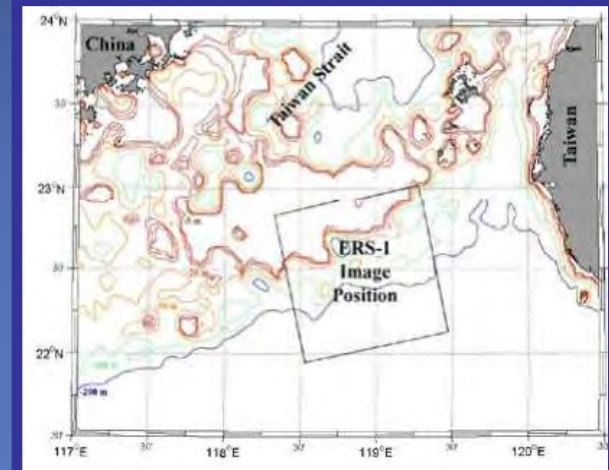
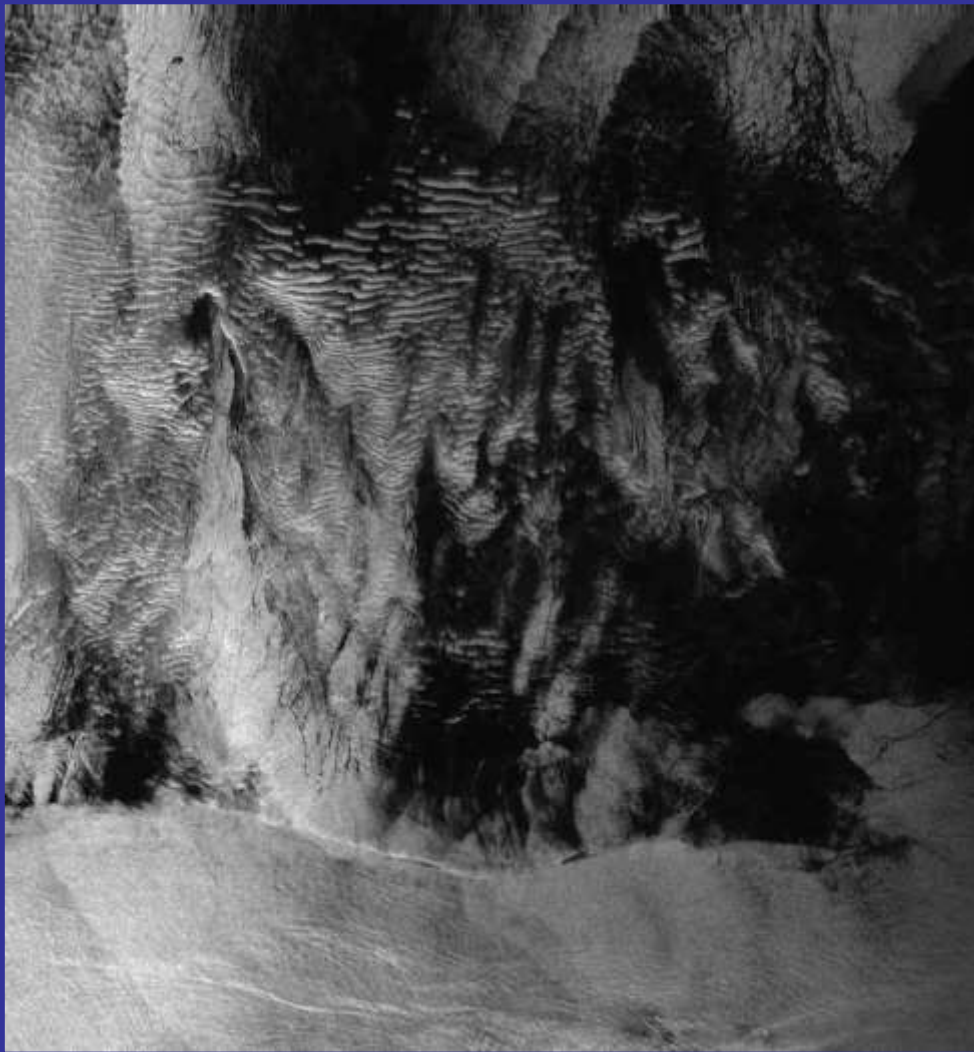
SAR Imaging of Sea Bottom Topography



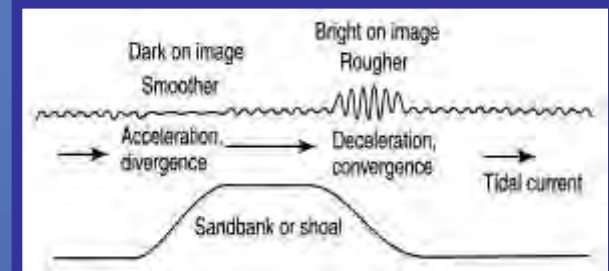
[Jackson & Apel, 2004]

Seasat SAR Image (L-HH, 100 km × 100 km)
English Channel
(August 1978, © NASA)

SAR Imaging of Sea Bottom Topography



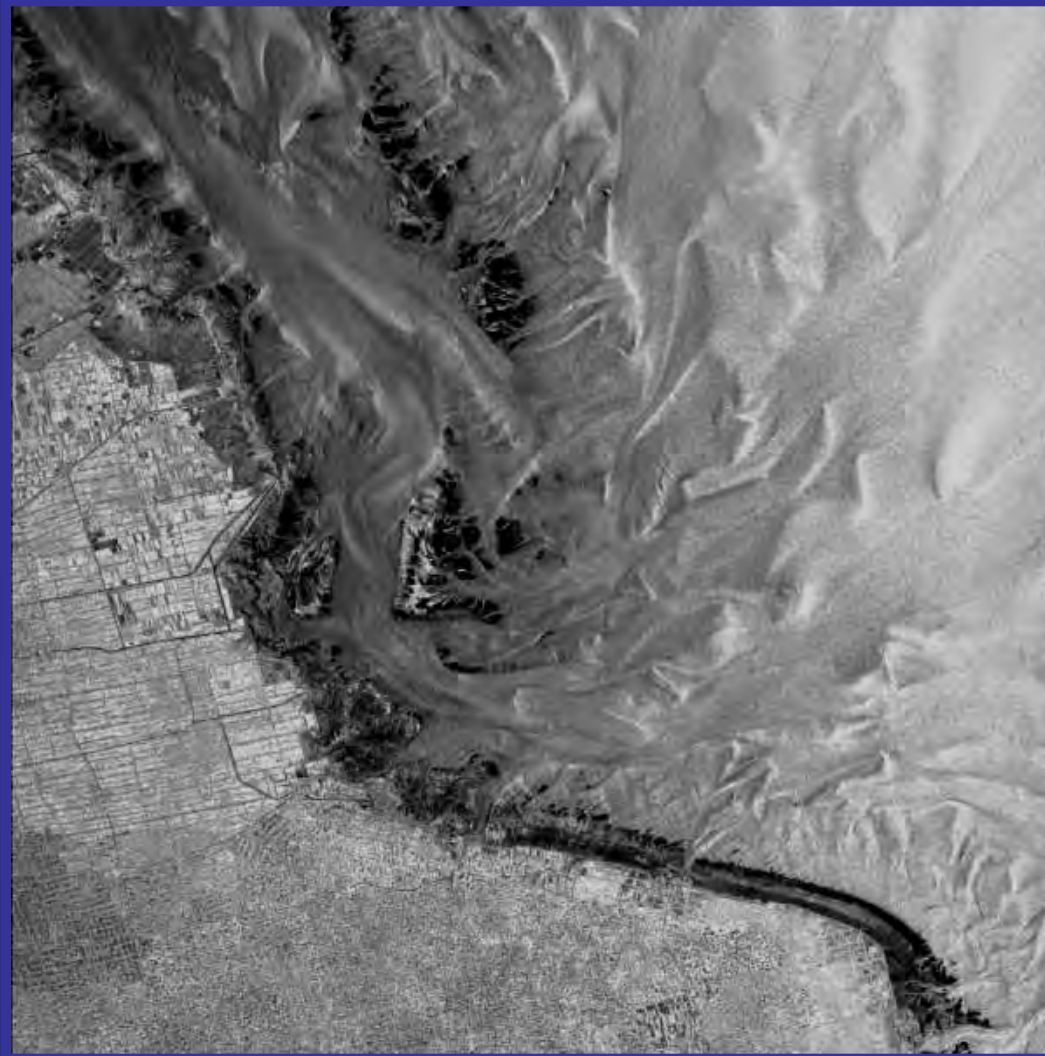
[Jackson & Apel, 2004]



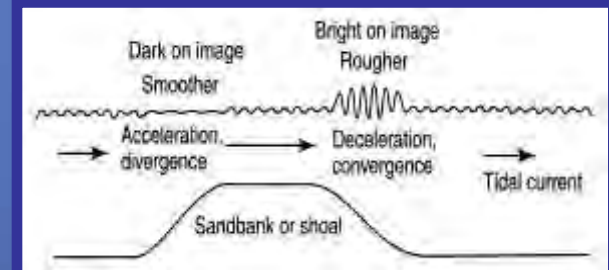
[Robinson, 2003]

ERS-1 SAR Image (C-VV, 100 km × 100 km)
Taiwan Tan Shoals
(27 July 1994, 14:31 UTC, © ESA)

SAR Imaging of Sea Bottom Topography



[Jackson & Apel, 2004]

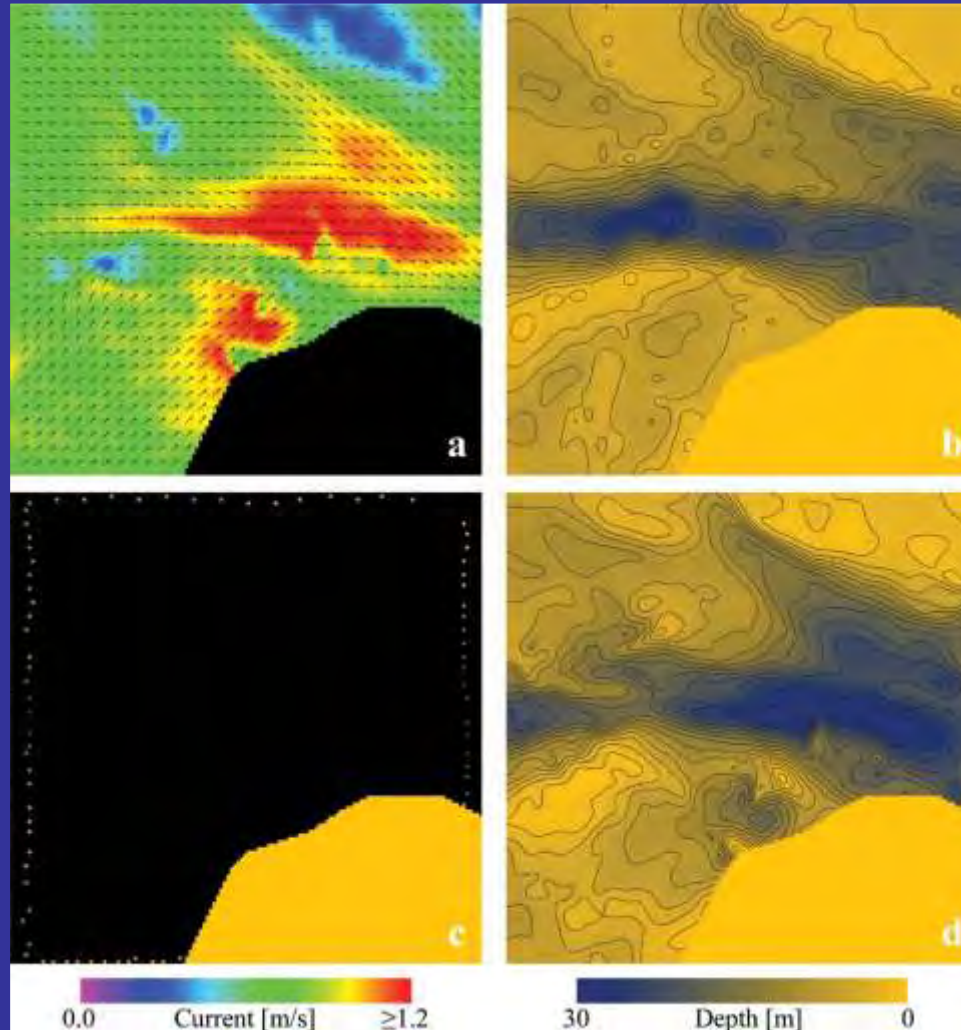


[Robinson, 2003]

ERS-1 SAR Image (C-VV, 100 km × 100 km)
Chinese Coast
(8 July 1995, 0234 UTC, © ESA)

Bathymetry Maps from ATI Measurements

Airborne ATI-derived
current vector field
(German island of Sylt,
experiments May 2001,
3.5 km × 3.5 km)



Depth map from
echosoundings

Selected reference
depth points

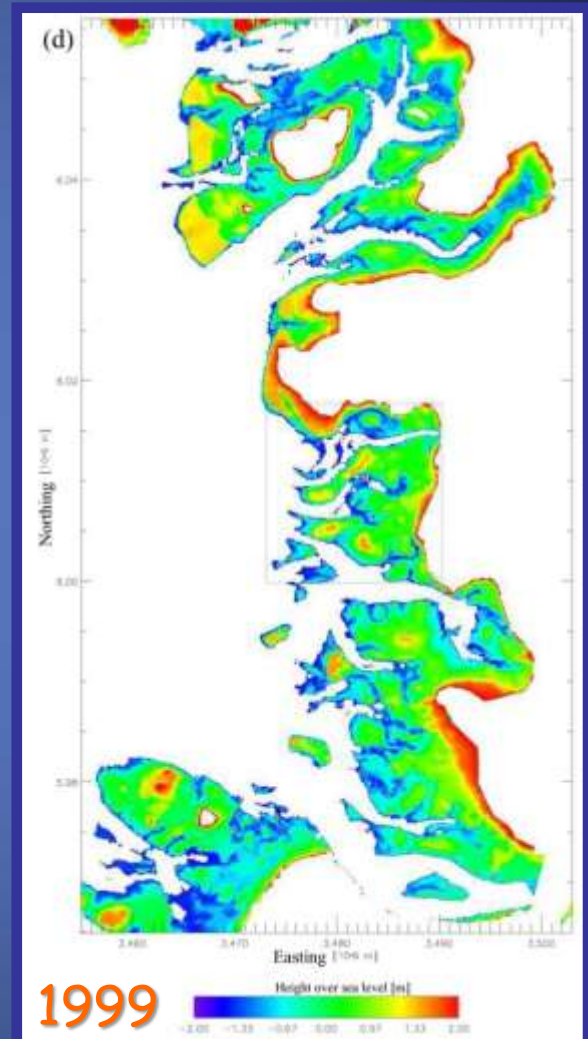
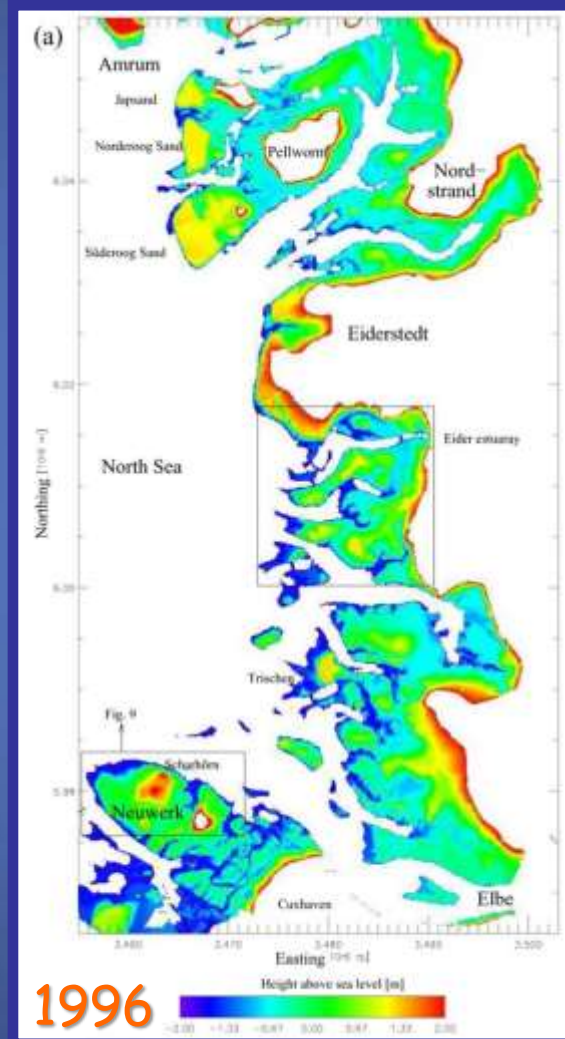
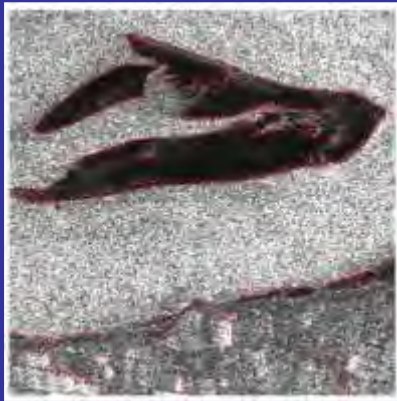
Depth map derived
from reference points

[Romeiser, 2013]

Bathymetry Maps from Multiple SAR Imagery

Waterline Method

Extract waterlines from multiple SAR images acquired at different tidal phases (precise water levels needed)



[Heygster et al., 2010]

Bathymetry Maps from Wave Statistics

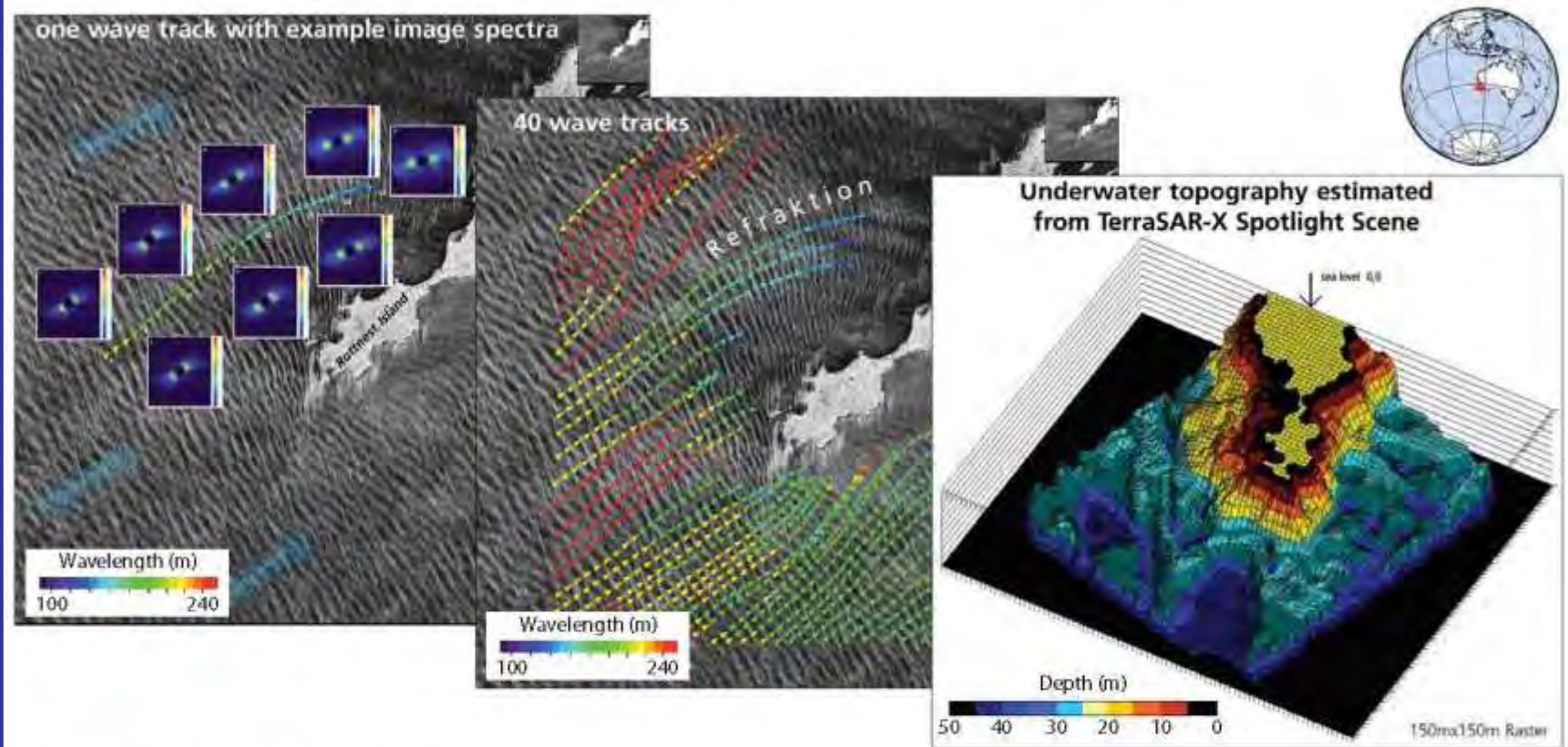


Figure 3. TerraSAR-X spotlight image (left) with dimensions of 10 km \times 10 km and resolution of 1 m acquired over Rottenest Island, Australia, on October 20, 2009. (left) Normalized radar cross section (NRCS) and one wave track with example image spectra. (center) Forty wave rays (colored lines) tracked on the image. (right) Bathymetry (uniform raster, 150 m resolution) estimated from the TerraSAR-X Image data. To complete the bathymetric maps in the shallowest areas (< 10 m water depth) near the coastline, optical data from the QuickBird satellite were used.

[Lehner et al., 2013]



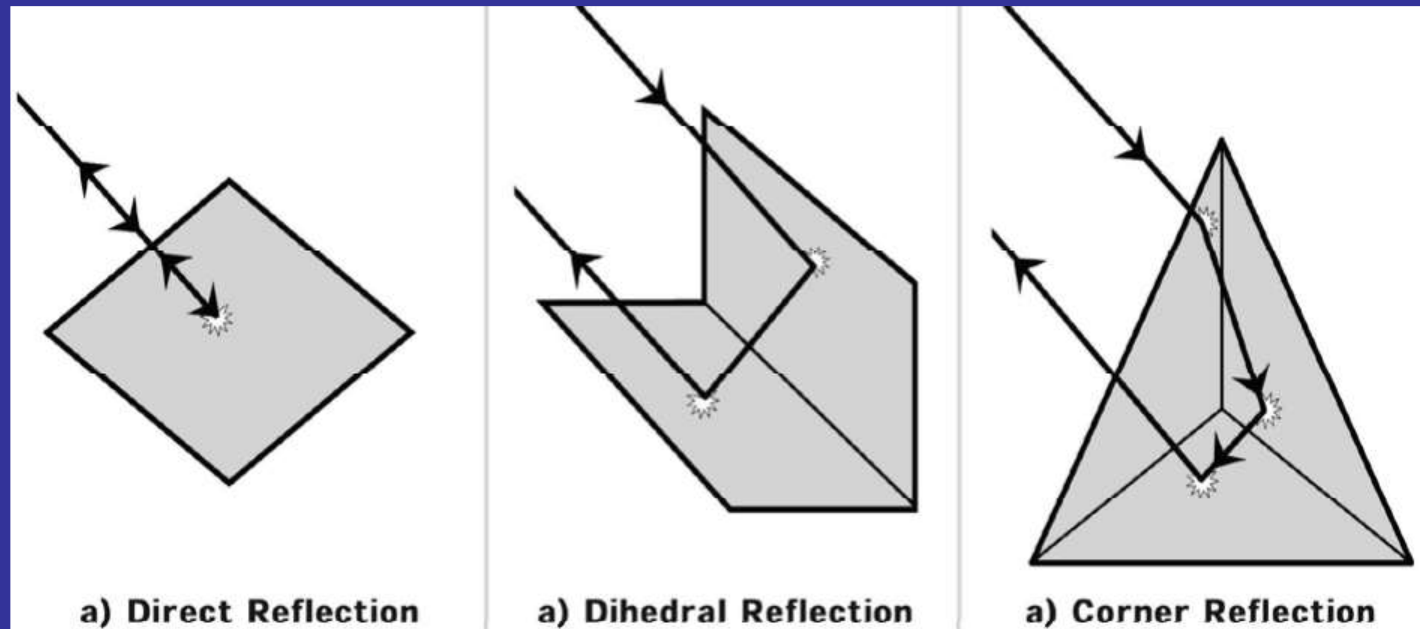
Sea Bottom Topography Take-Home Messages

Current variations: roughness variations
Current models (shallow waters)
Waterline method (intertidal flats)
Wave refraction (coasts)



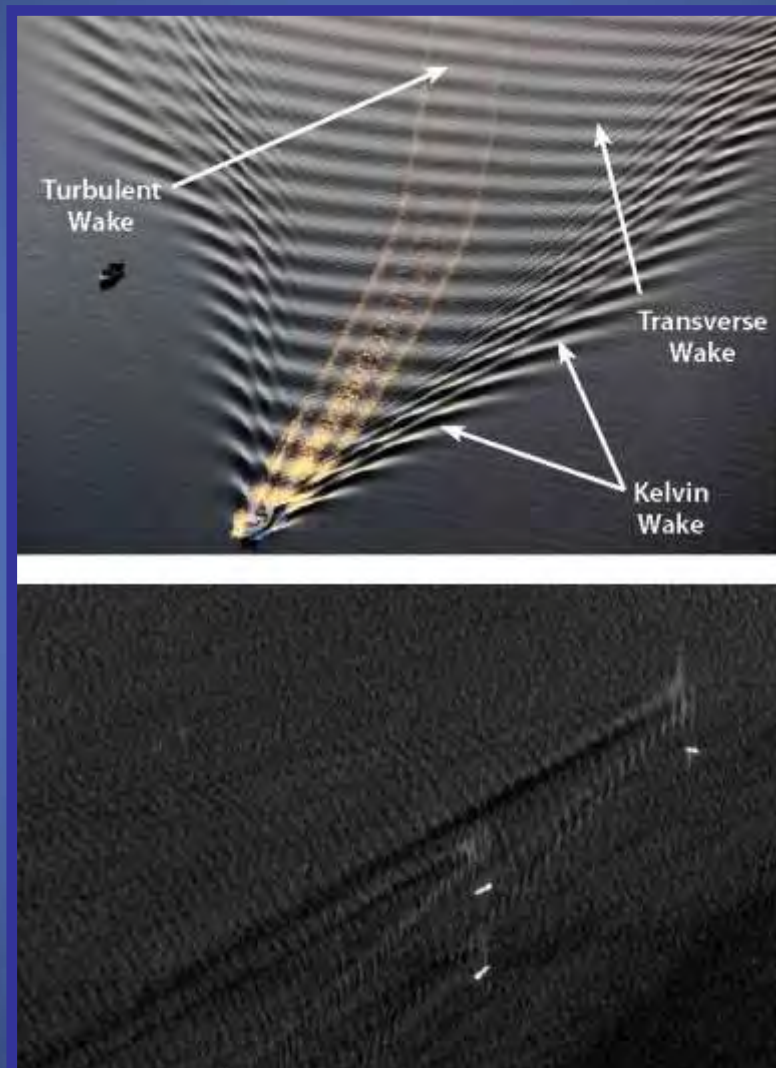
Ship Detection

Radar Backscattering from Metal Constructions



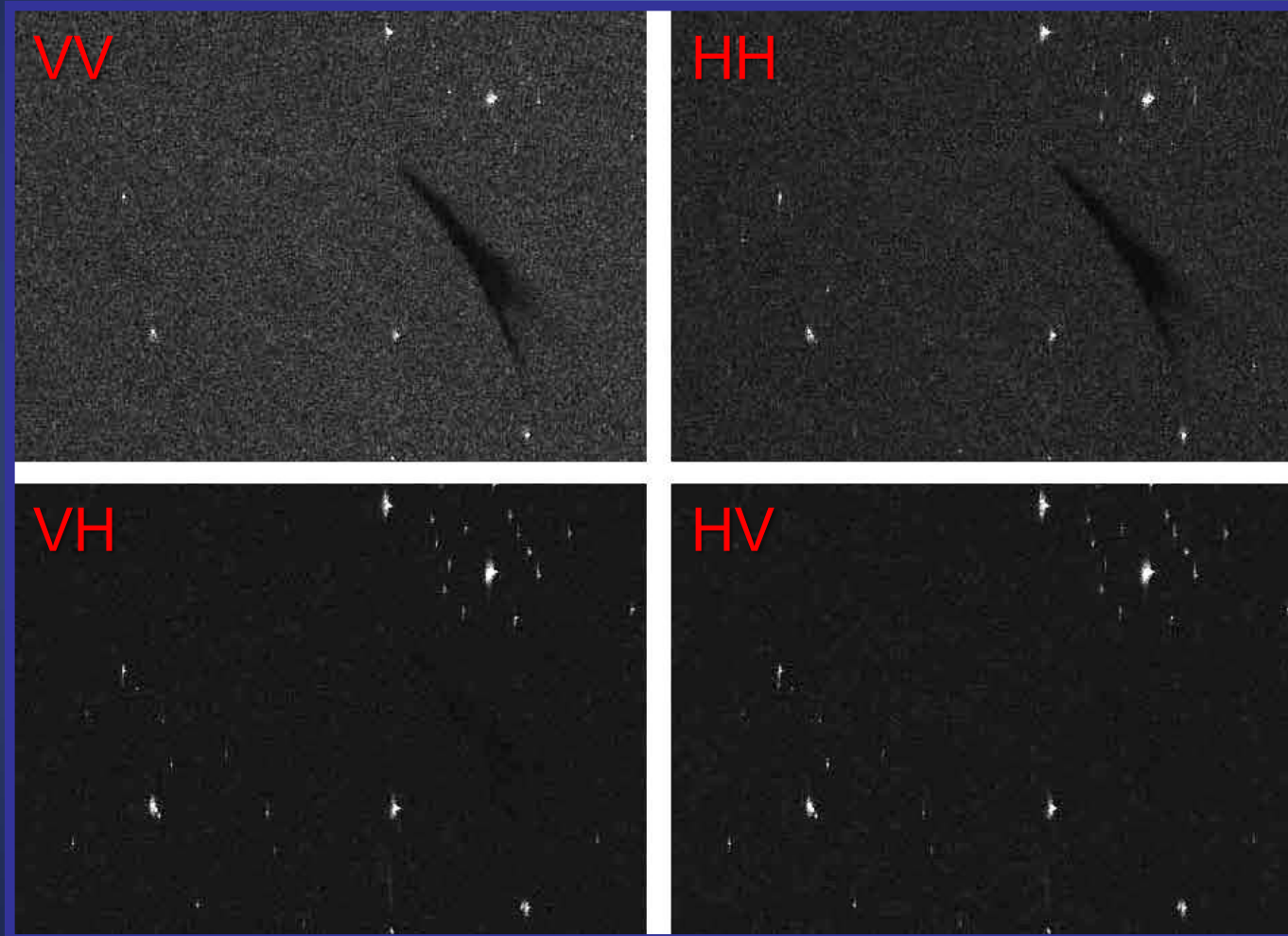
[Jackson & Apel, 2004]

Ship Wakes



[Mallas & Graber, 2013]

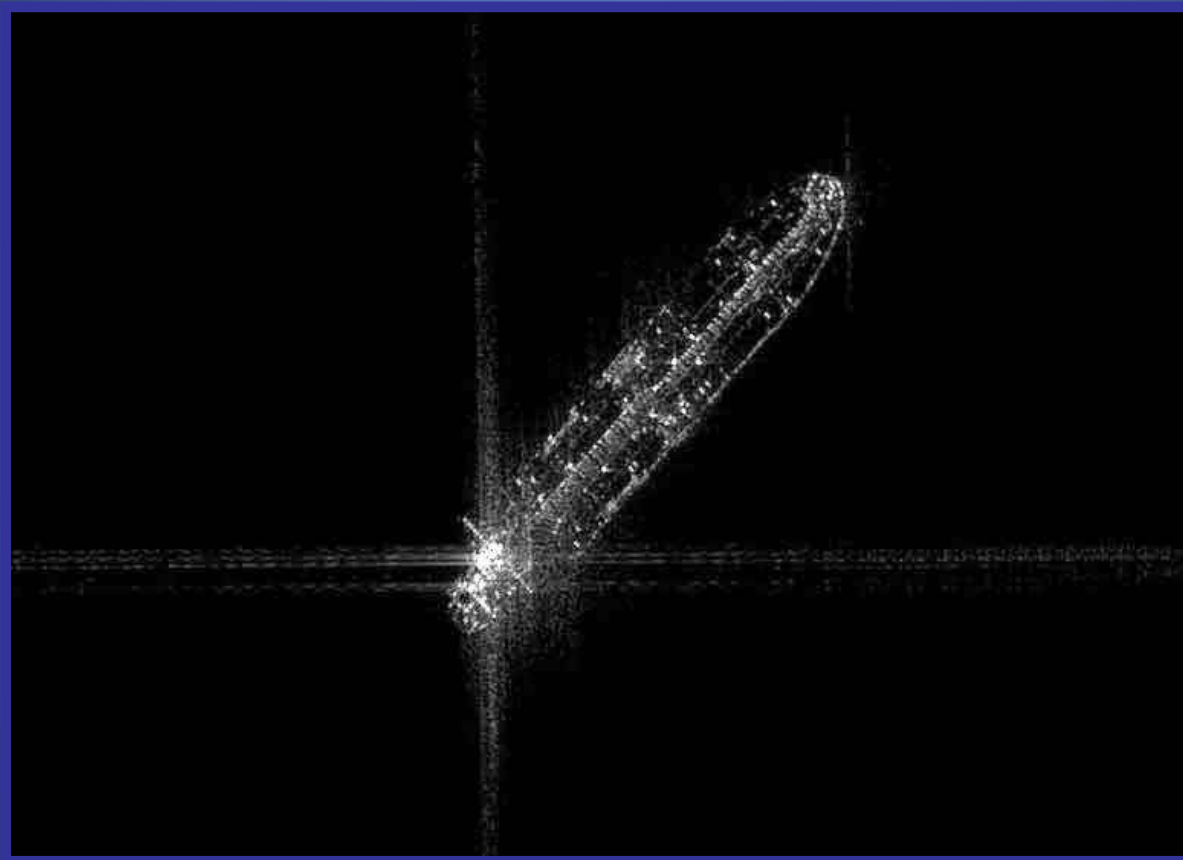
Multi-Polarization SAR Imaging of Vessels



Radarsat-2 SAR
Imagery (C), © CSA

[Mallas & Graber, 2013]

High-Resolution SAR Imaging of Large Vessels



COSMO-SkyMed
SAR Image (X-VV)
© COSMO-SkyMed

[Mallas & Graber, 2013]

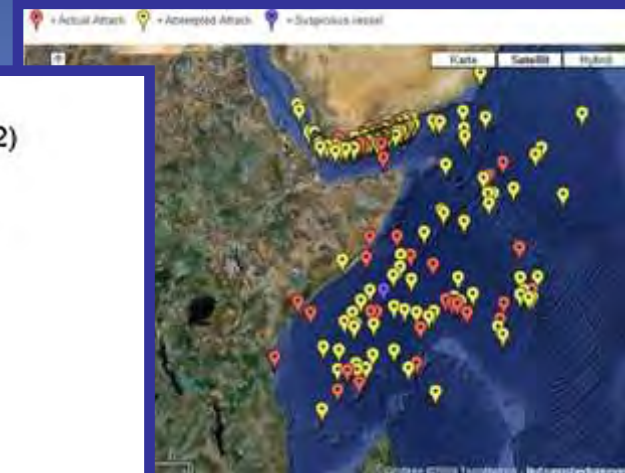
SAR Imaging of Hijacked Vessels



Izumi (1)
Golden Wave (2)
MV York (3)
are detected

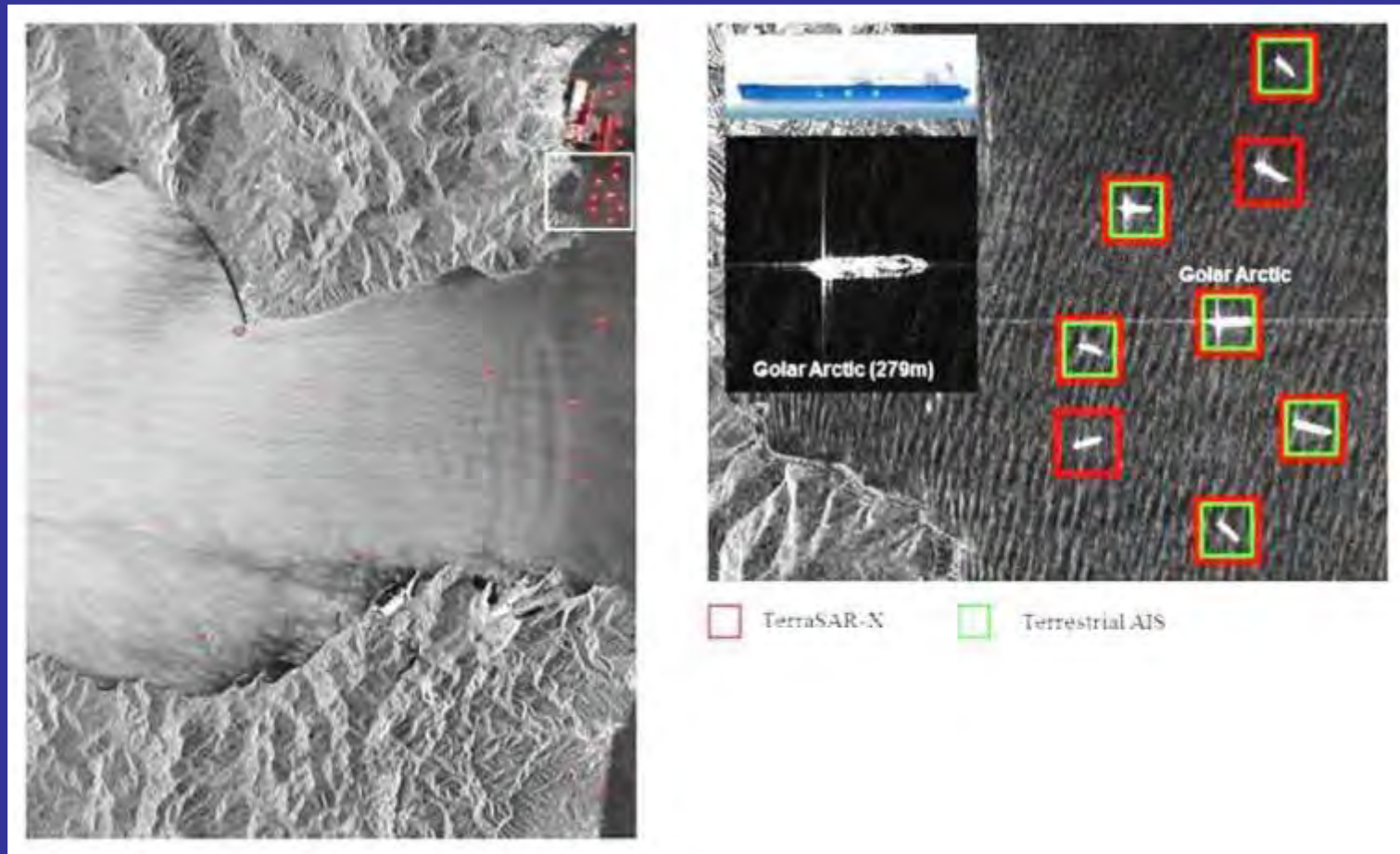


Izumi (1), Golden Wave
and (2) and MV York (3)
are detected and 2 more
Objects (small boats) have
been detected:
(4) 23m length,
(5) 9m length



[Barale & Gade, 2014]

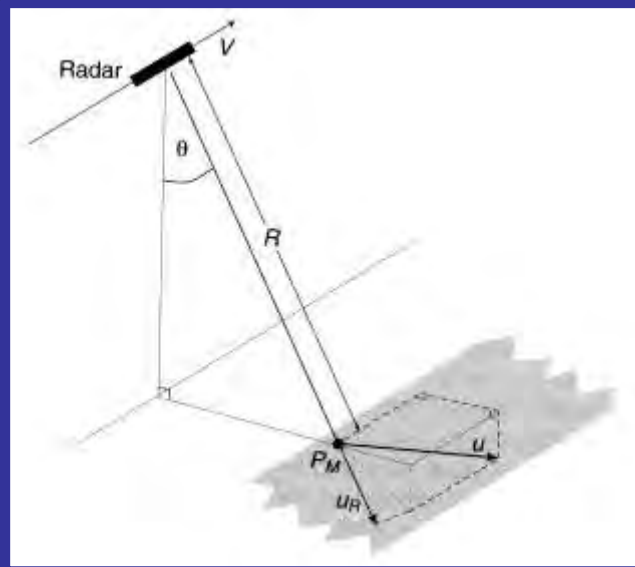
SAR Imaging of Vessels vs. AIS Info



[Barale & Gade, 2014]

SAR Imaging of Marine Vessels

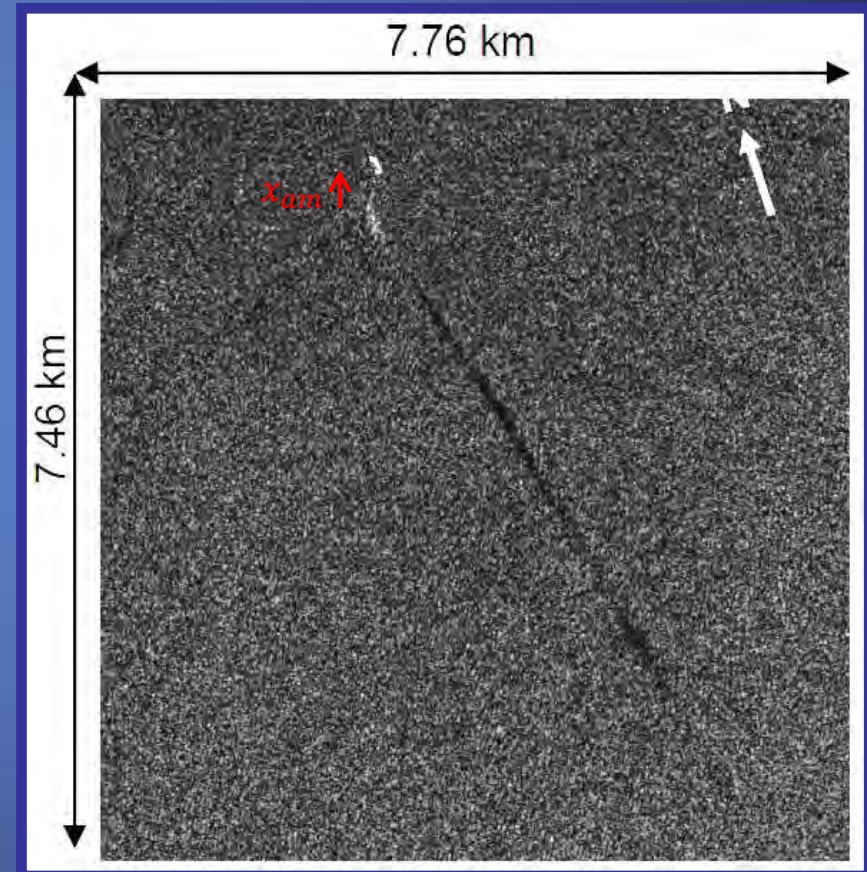
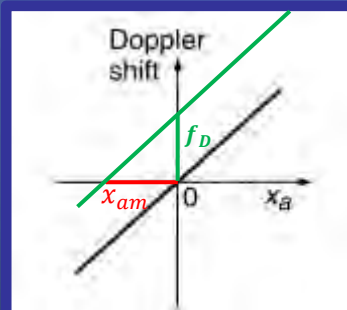
Speed estimate from azimuthal shift



[Robinson, 2003]

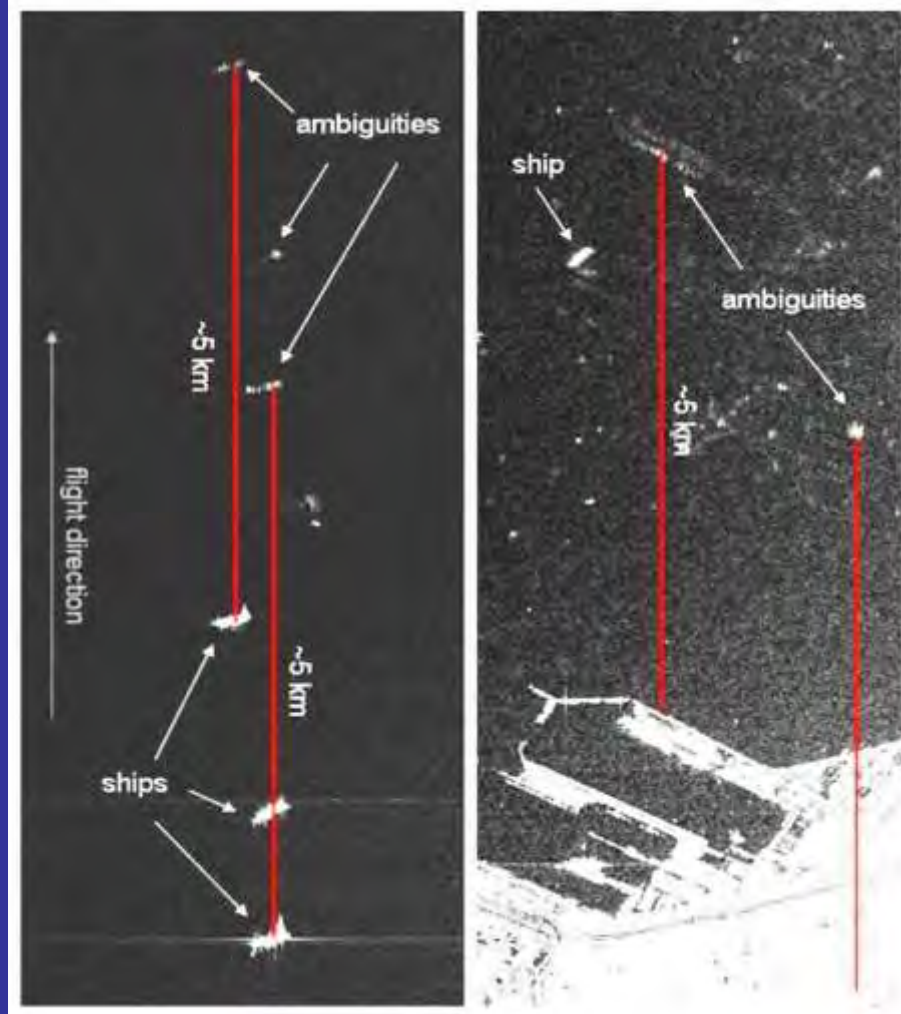
$$f_D = -\frac{2u_R}{\lambda}$$

$$x_{am} = -\frac{u_R R}{V}$$



[Soloviev et al., 2008]

SAR Ambiguities ('Ghost Images')



Ambiguity distance:

$$\Delta x = \Delta t_{AMBI} \cdot v_0 = \frac{PRF}{FM} \cdot v_0$$

PRF : pulse repetition frequency

FM : temporal derivative of Doppler frequency

v_0 : zero Doppler velocity

TerraSAR-X: $\Delta x \approx 5.2$ km

[Barale & Gade, 2014]



Ship Detection Take-Home Messages

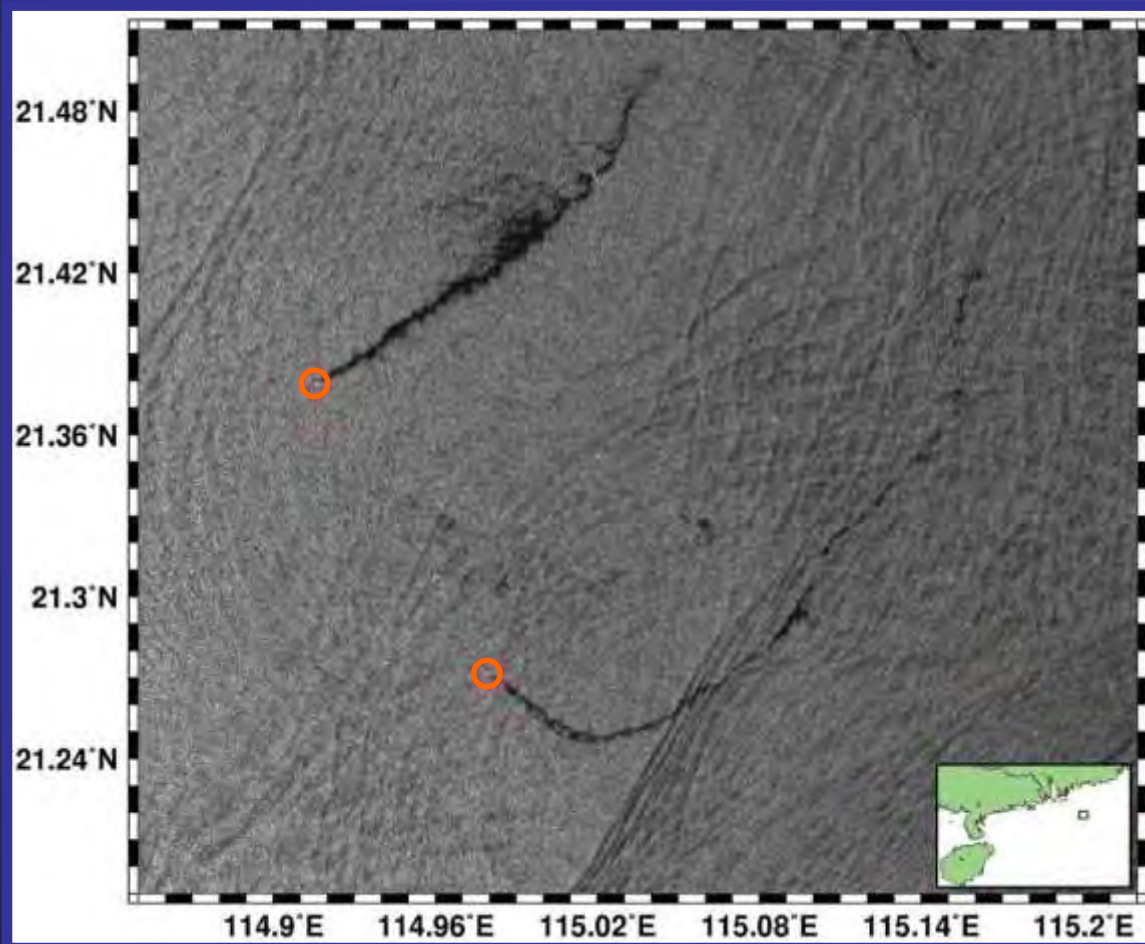
High-resolution SAR used
Vessel monitoring (SAR vs. AIS)
Vessel speeds ("ship-off-the-track")



Oil Pollution Monitoring

SAR Monitoring of Marine Oil Pollution

Operation Oil Pollution

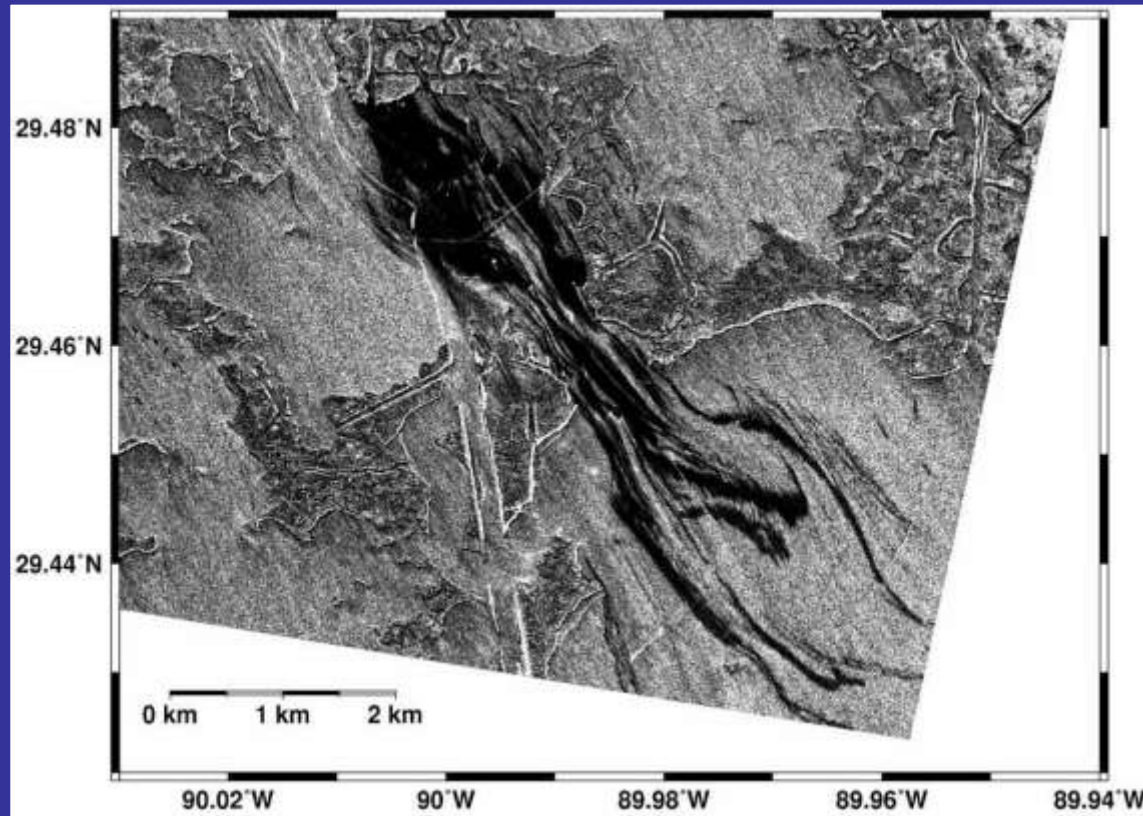


ERS SAR Image (C-VV, 50 km × 50 km)
South China Sea
(25 May 2007, 14:44 UTC, © ESA)

[Caruso et al., 2013]

SAR Monitoring of Marine Oil Pollution

Accidental Oil Pollution



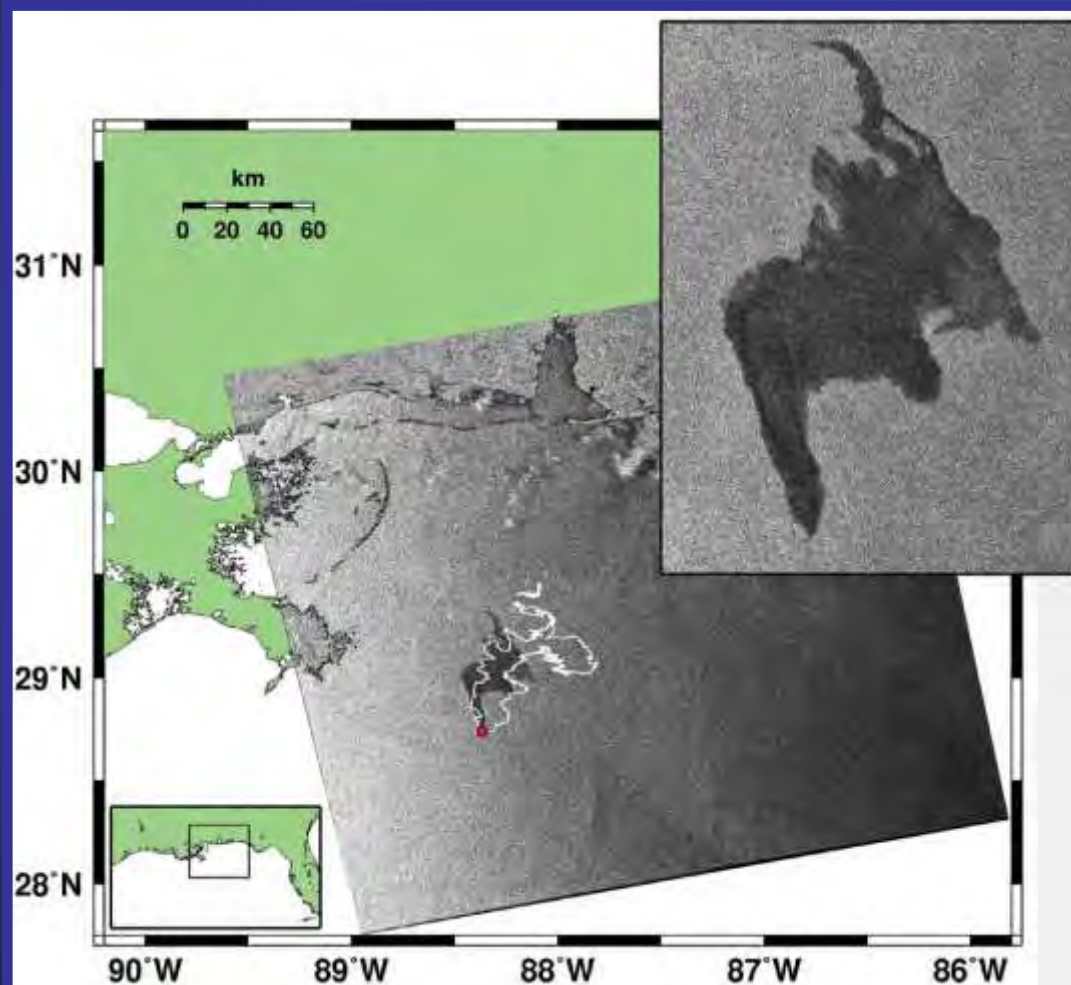
Wellhead struck by tugboat *Pere Ana C.*

TerraSAR-X Image (X-VV)
Mud Lake, LA, USA
(1 August 2010, 12:08 UTC, © DLR)

[Caruso et al., 2013]

SAR Monitoring of Marine Oil Pollution

Accidental Oil Pollution



Deepwater Horizon (●) incident

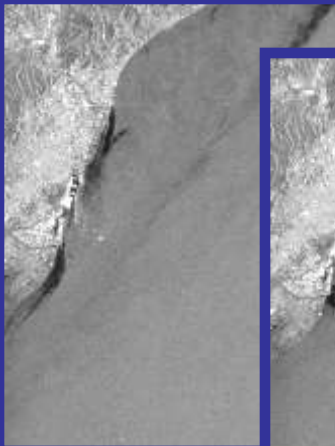
TerraSAR-X Image (X-VV)
Gulf of Mexico
(23 April 2010, 12:08 UTC, © DLR)

Extent on 25 April 2010:

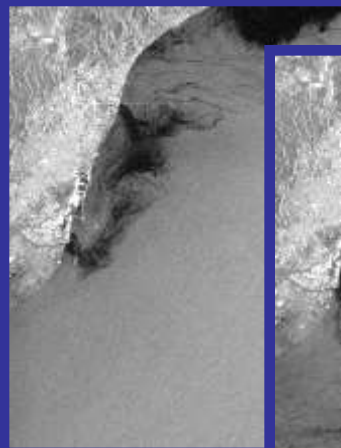


[Caruso et al., 2013]

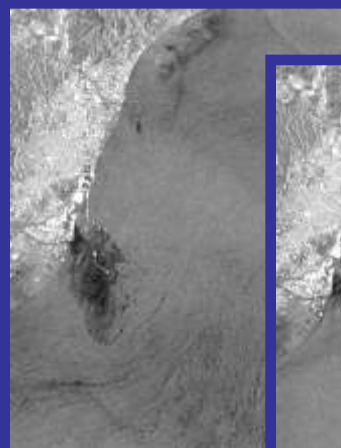
SAR Image Examples



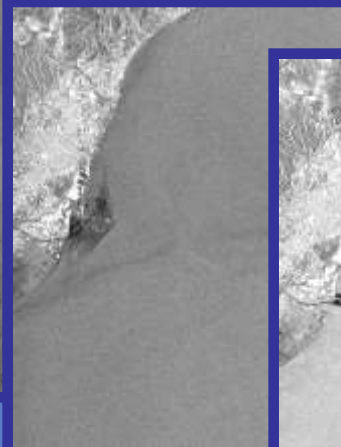
11 January 1998



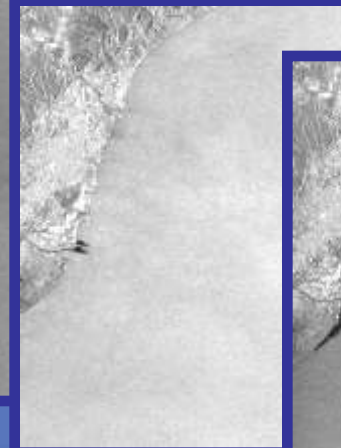
15 February 1998



31 May 1998



5 July 1998



2 October 1998



18 October 1998

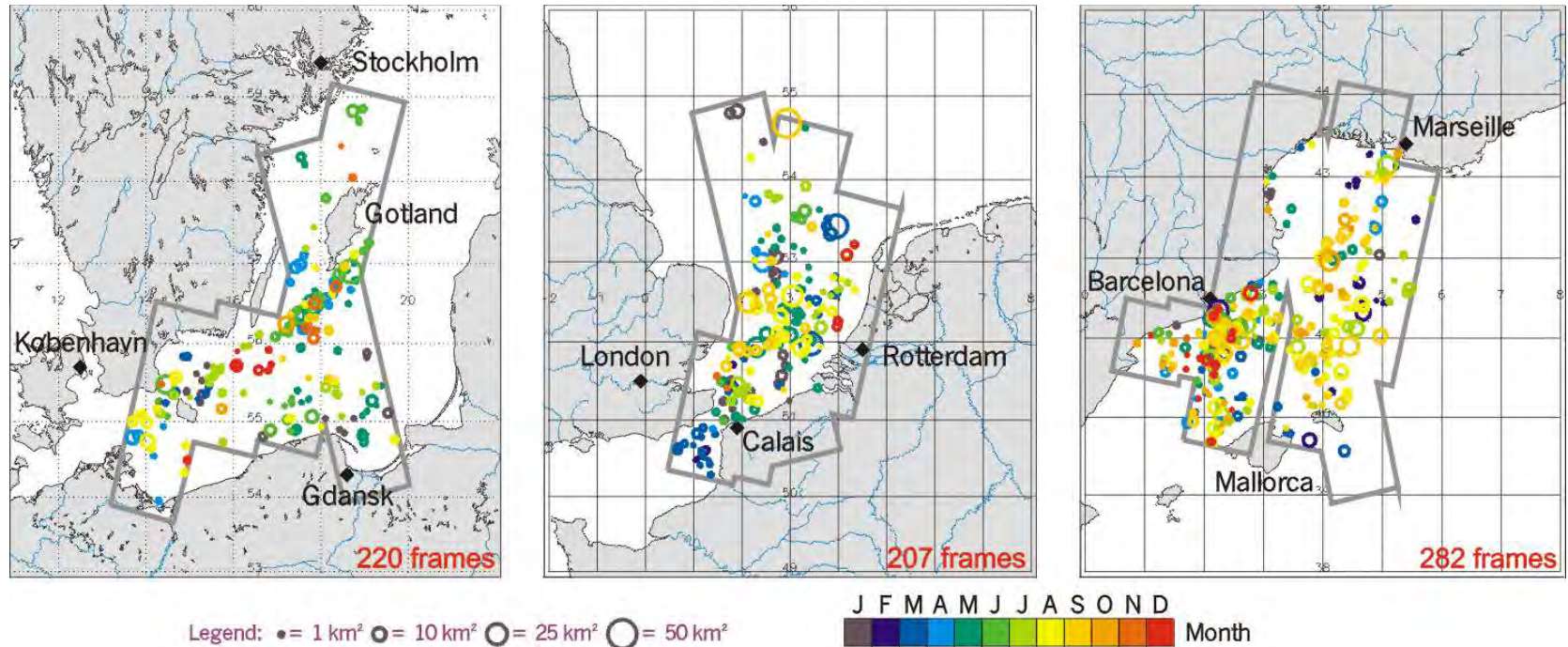
(30 km × 40 km)



ERS-2 SAR Images (C-VV, 30 km × 40 km)
Northwestern Mediterranean Sea
(© ESA)

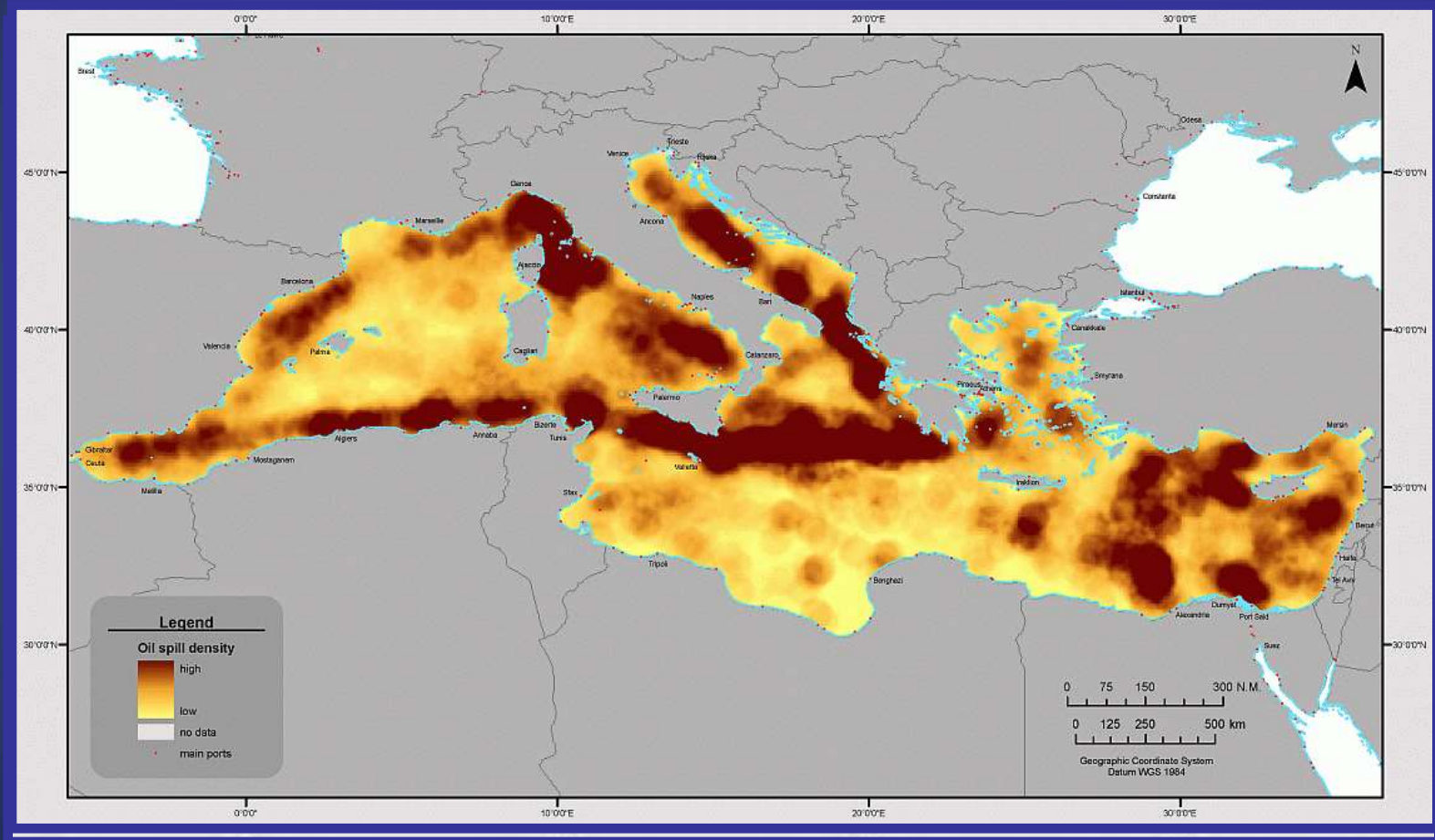
SAR Applications

Oil pollution in European marginal seas (1996-99)



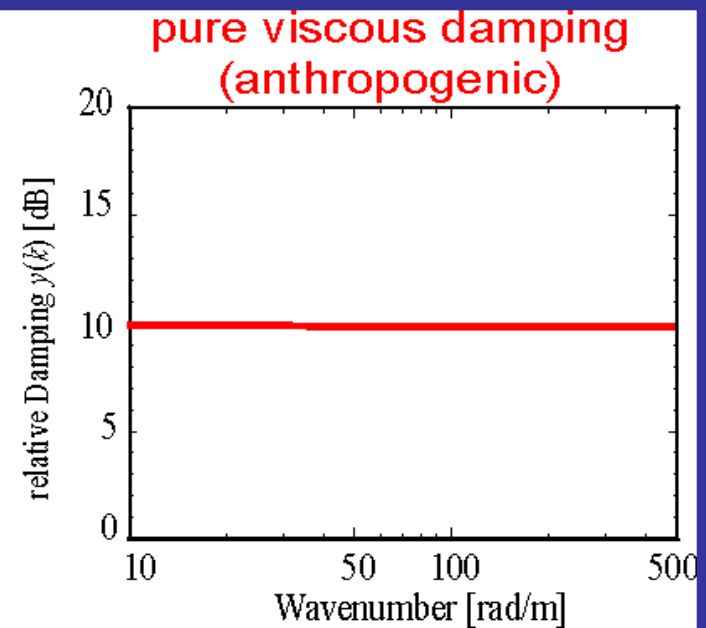
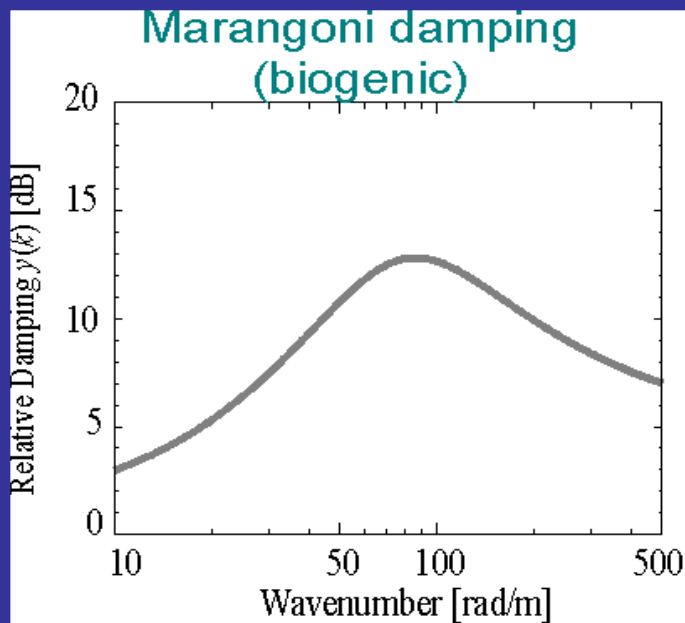
SAR Applications

Mean oil pollution of the Mediterranean Sea 1999-2004

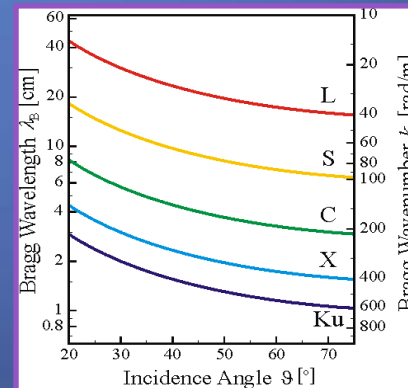


[Barale & Gade 2008]

Wave Damping by Surface Films



Use multi-frequency radar techniques to discriminate between biogenic and anthropogenic surface films



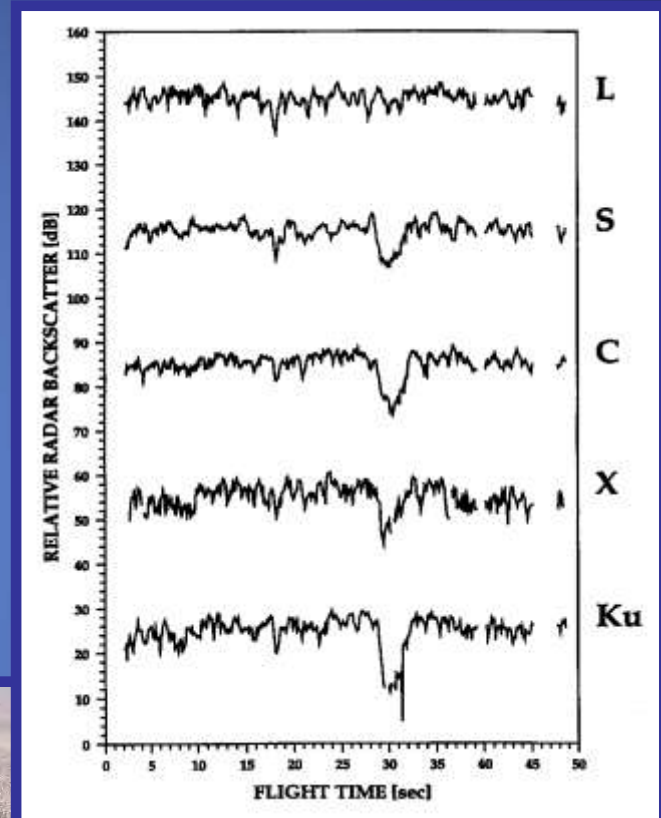
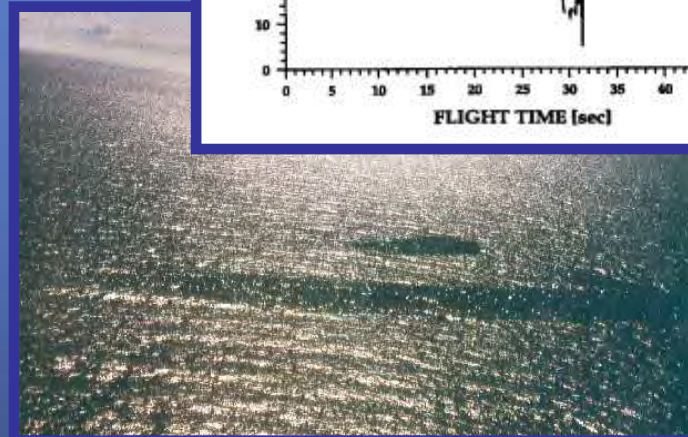
Scatterometer Experiments



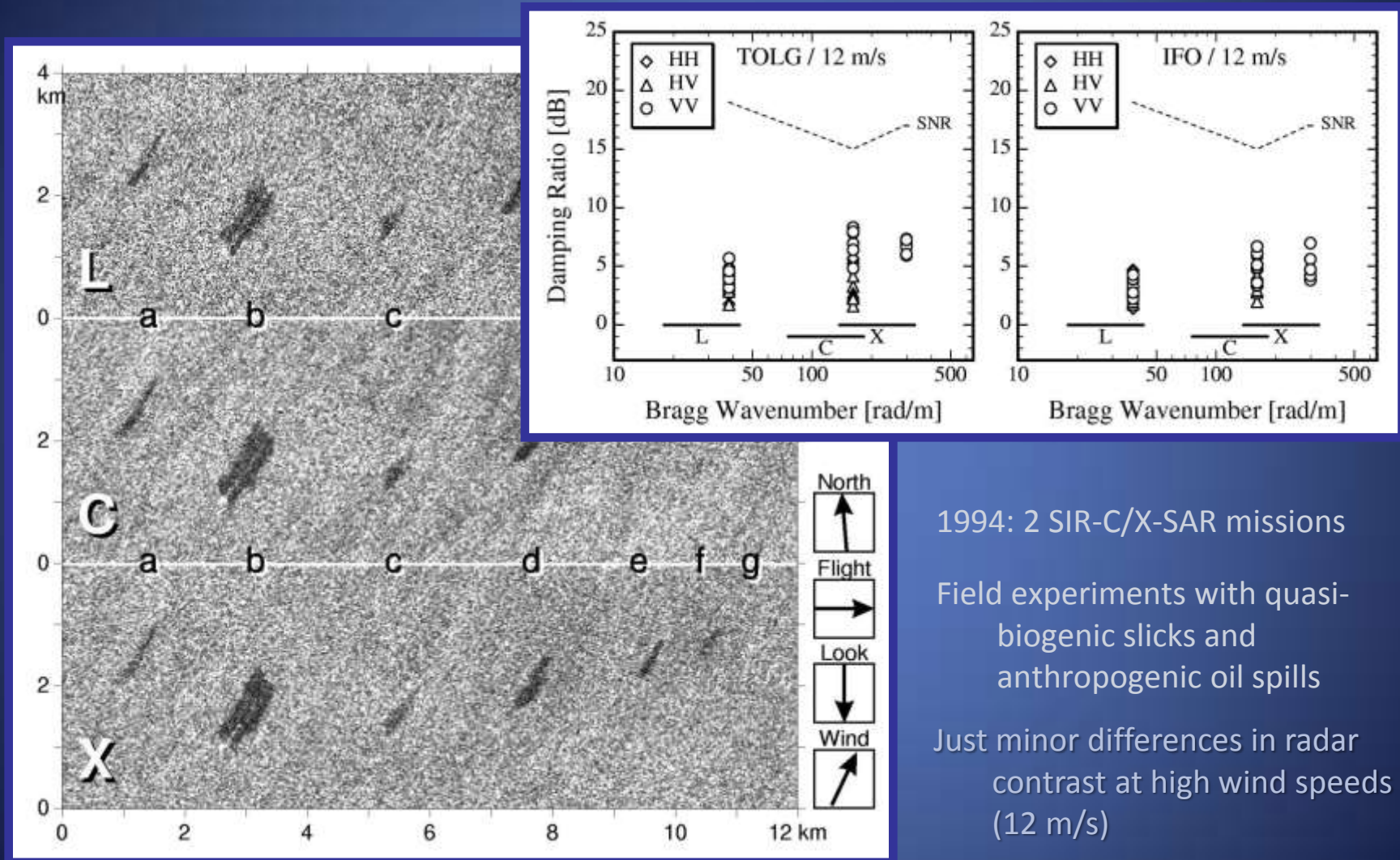
MULTI³SCAT of Uni Hamburg

- flown on BO 105
- 5 frequencies: (L, S, C, X, Ku band)
- 4 polarisations (HH, HV, VV, VH)
- incidence angle: 23° ... 65°
- nominal flight height: 150 m
- Ø footprint: 1.6 m ... 128.9 m
- transmit power: 10 mW ... 150 mW

Field Experiments With Marine Surface Films



Field Experiments With Marine Surface Films



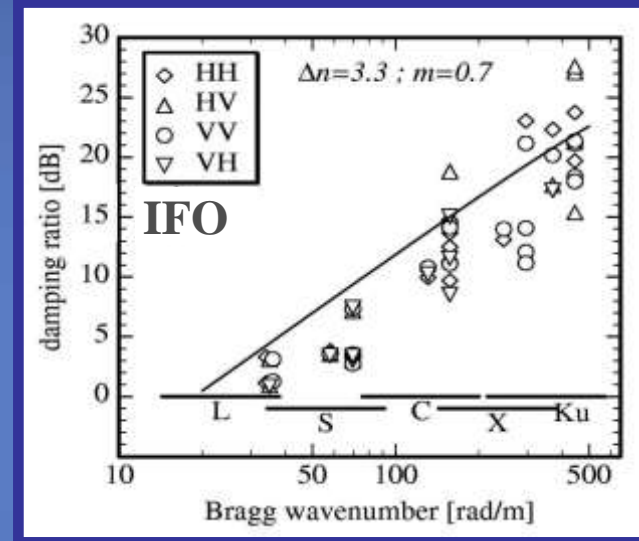
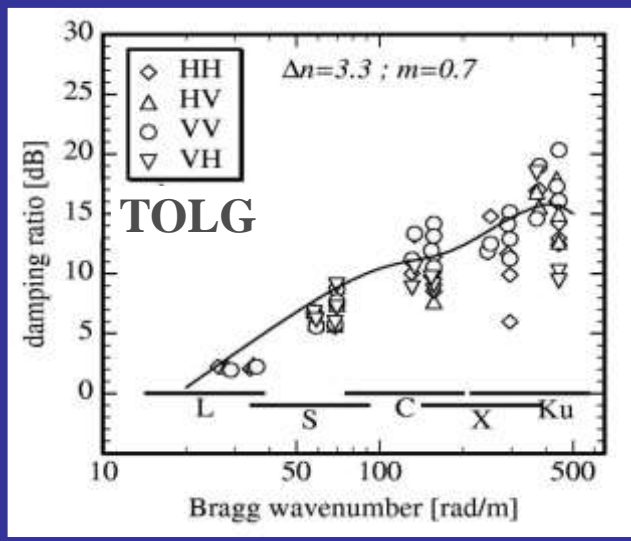
1994: 2 SIR-C/X-SAR missions

Field experiments with quasi-biogenic slicks and anthropogenic oil spills

Just minor differences in radar contrast at high wind speeds (12 m/s)

Field Experiments With Marine Surface Films

Modeling damping ratios at high wind speeds



[Gade, 1996]

$$\frac{\sigma^{(0)}}{\sigma^{(s)}} = \frac{\Psi_0(k)}{\Psi_s(k)} \approx \frac{\beta_s - 2\Delta_s c_g}{\beta_0 - 2\Delta_0 c_g} \cdot m^{\Delta n - 4} \left(2u_* \sqrt{\frac{|\cos \varphi| k}{g}} \right)^{\Delta n}$$

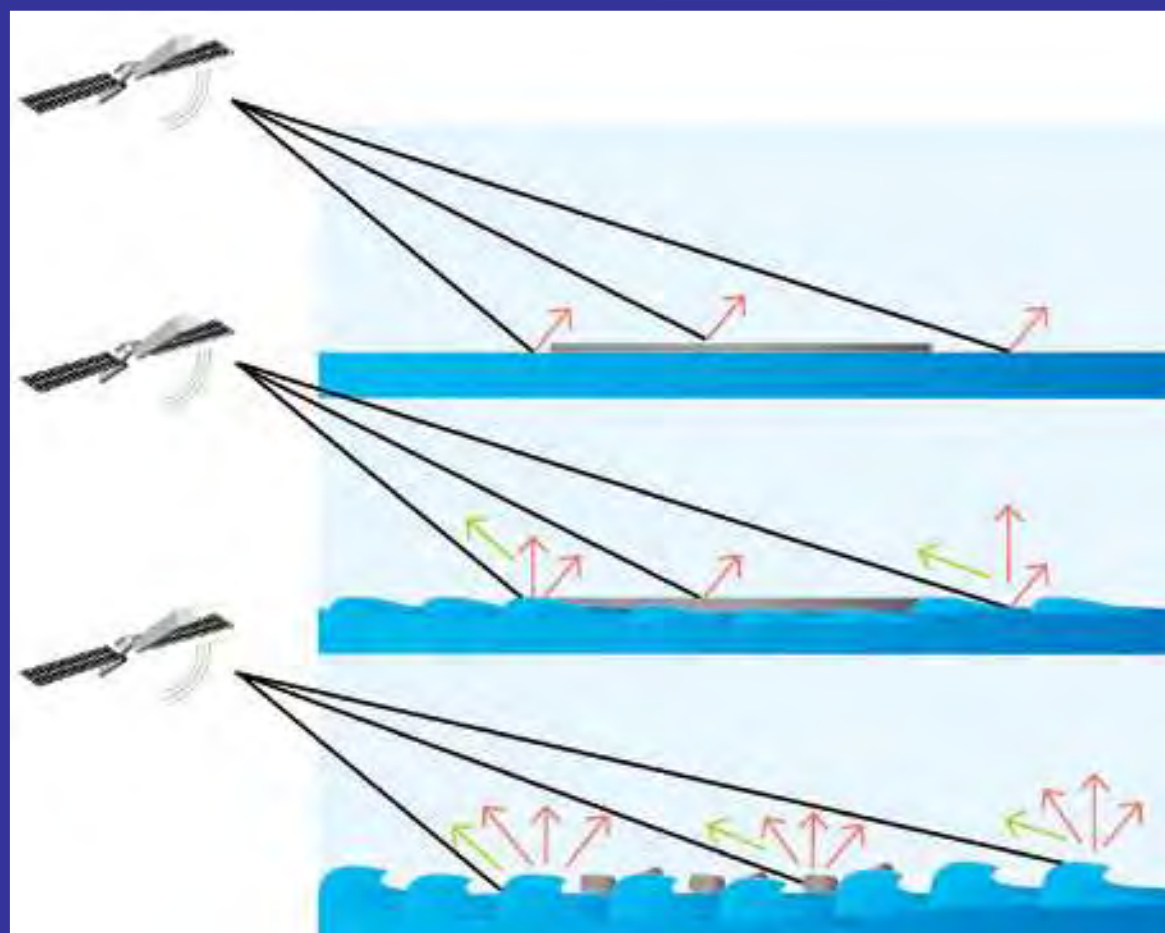
m : parameter describing reduction of friction velocity
 Δn : parameter describing reduction of wave breaking

Model can explain

monotonous increase of
 damping curves (no Marangoni
 maximum!)

similar damping behavior
 of biogenic and anthropogenic
 films

SAR Oil Detection System



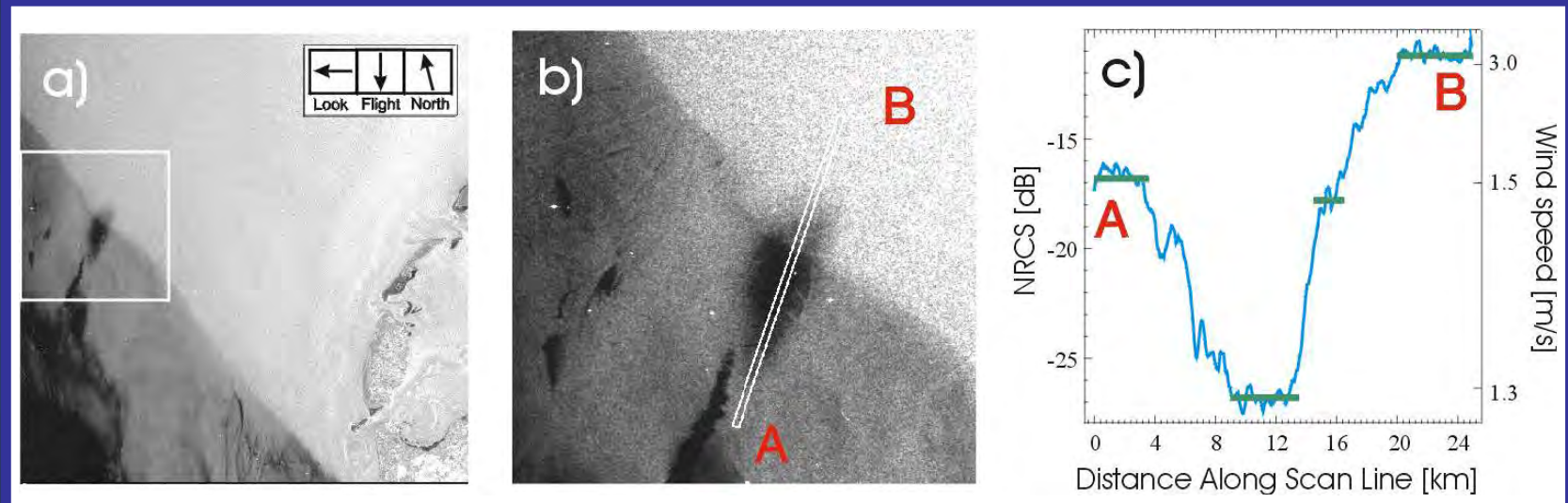
Low wind

Moderate wind

High wind

[EMSA, 2014]

Wind-Speed Dependence of Radar Contrast

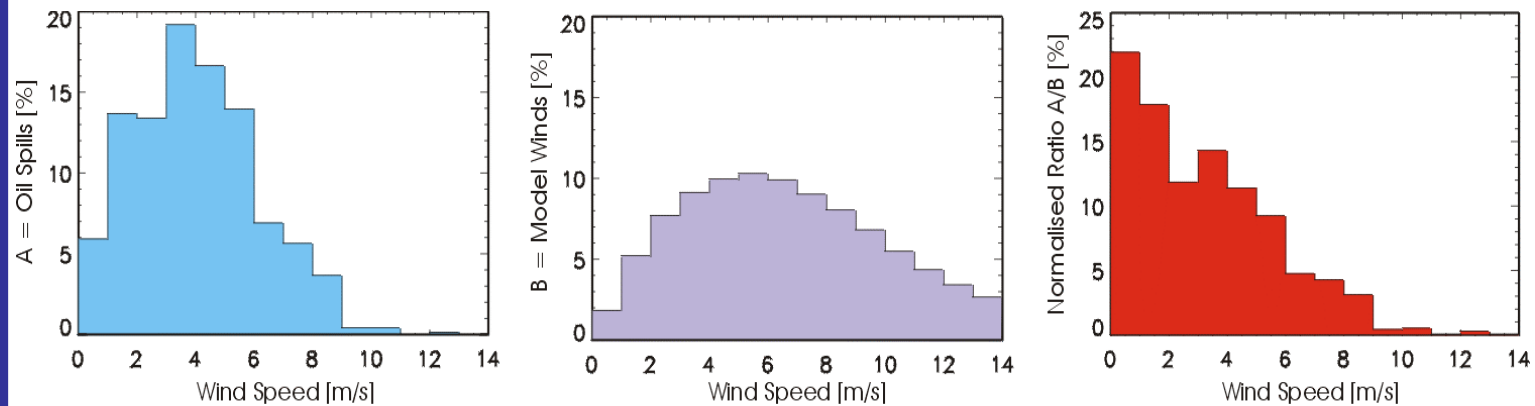


ERS-2 SAR image (C-VV, 100 km 100 km)
North Sea
24 March 1997, 10:40 UTC, © ESA

Statistical Analyses

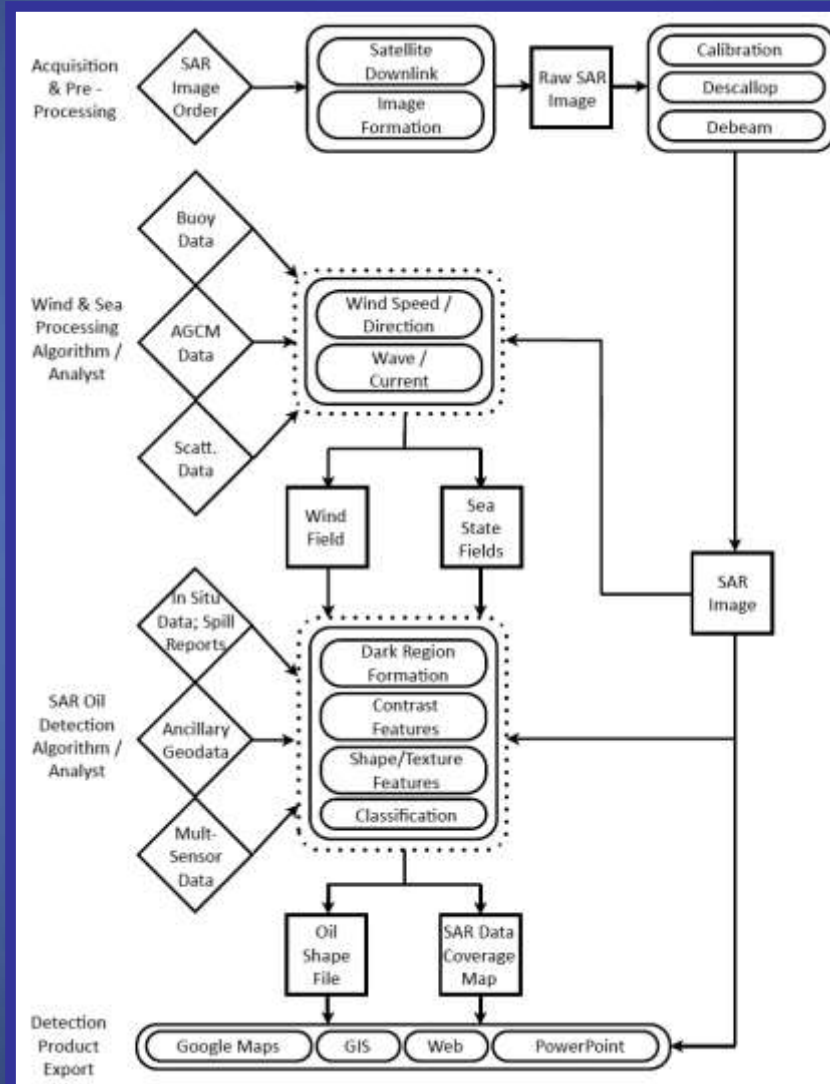
Normalized Visibility

Defined as ratio A/B of the wind speed distribution of detected oil spills (A) and model winds (B)



Any oil pollution in the three 'Clean Seas' test sites is visible only at wind speeds up to 9-10 m/s !

SAR Oil Detection System



[Caruso et al., 2013]



Oil Pollution Monitoring Take-Home Messages

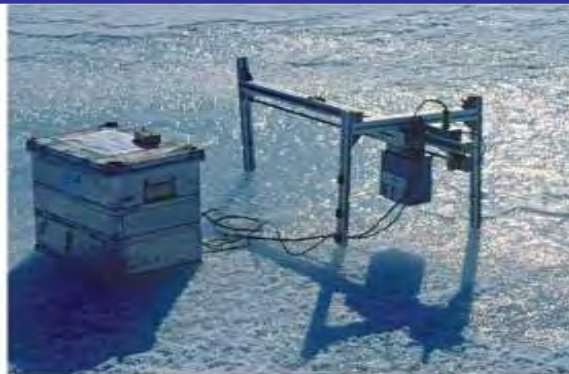
Routine monitoring, pollution statistics
Oil-cleanup support
Detection @ 2 m/s - 10 m/s



Sea Ice

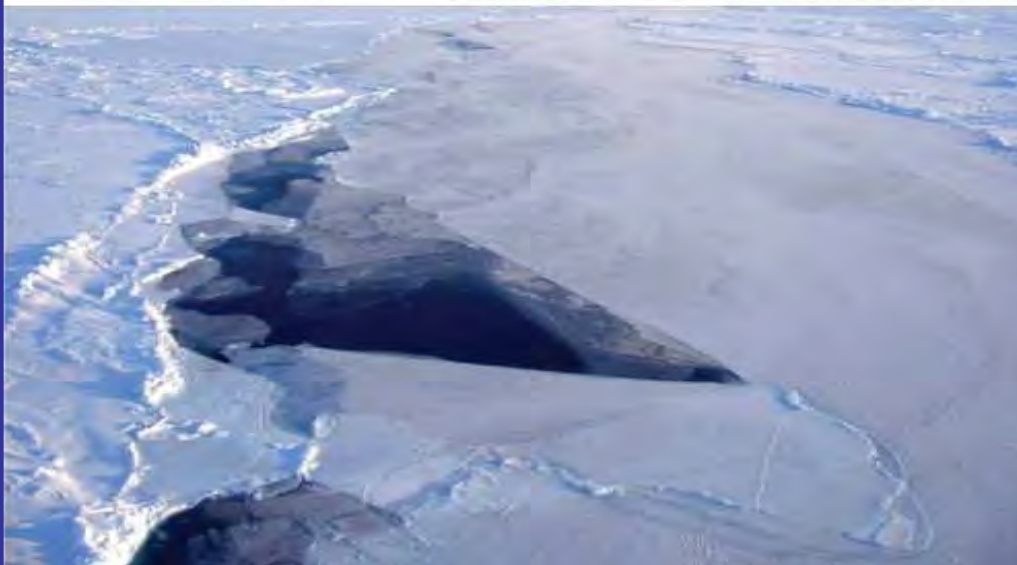
Sea Ice

Roughness scales and volume inclusion



Left: Air bubbles in Baltic first-year ice (ice slab diameter 8 cm)

Right: Small-scale ripples on sea ice (laser measurements in the Baltic)

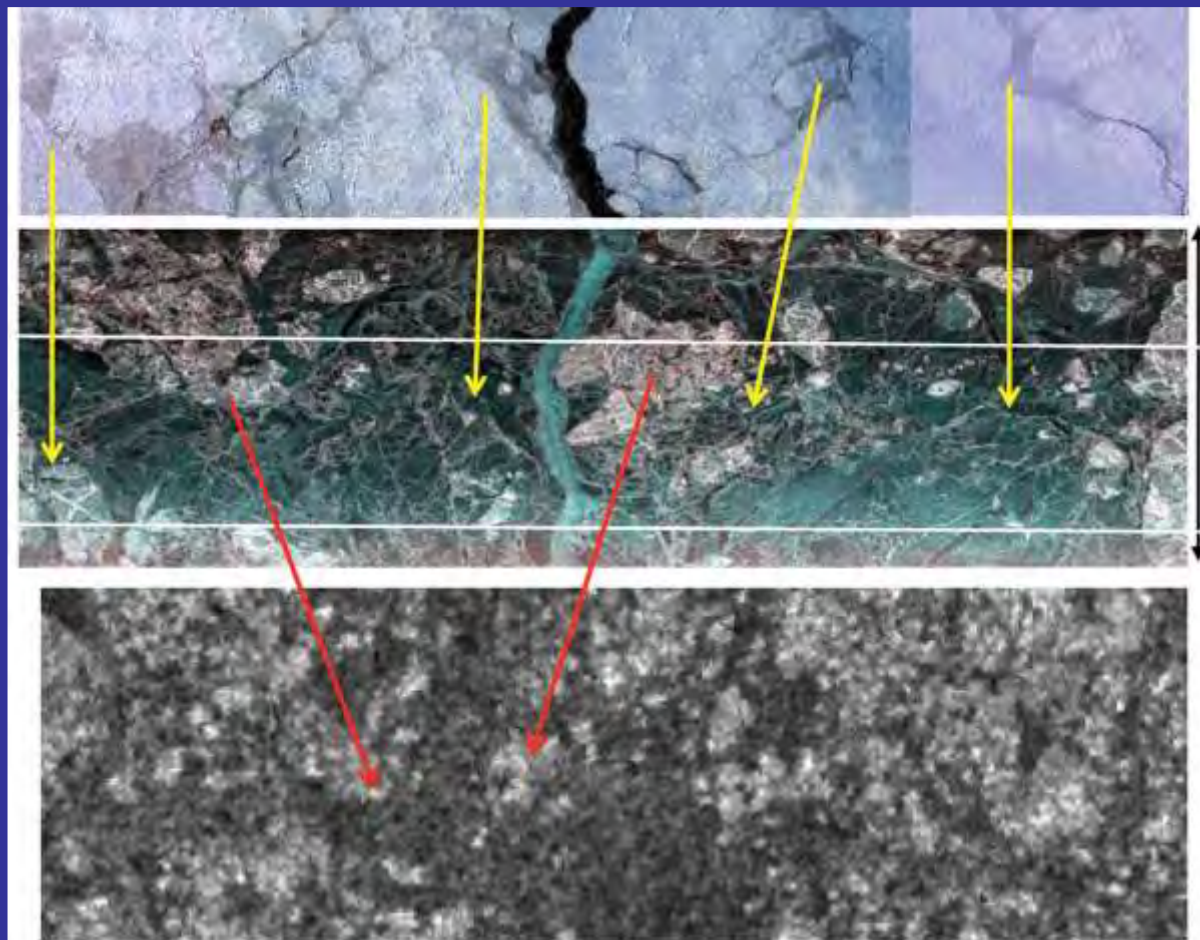


Left: Deformed sea ice in the Fram Strait (refrozen lead with rafted thin ice; thicker, ridged ice)

[Dierking 2013]

Remote Sensing of Sea Ice

Comparison of optical and SAR imagery (N Svålbard)



Airborne optical imager
19 March 2007, 12:20 UTC
spatial resolution < 1.3 m

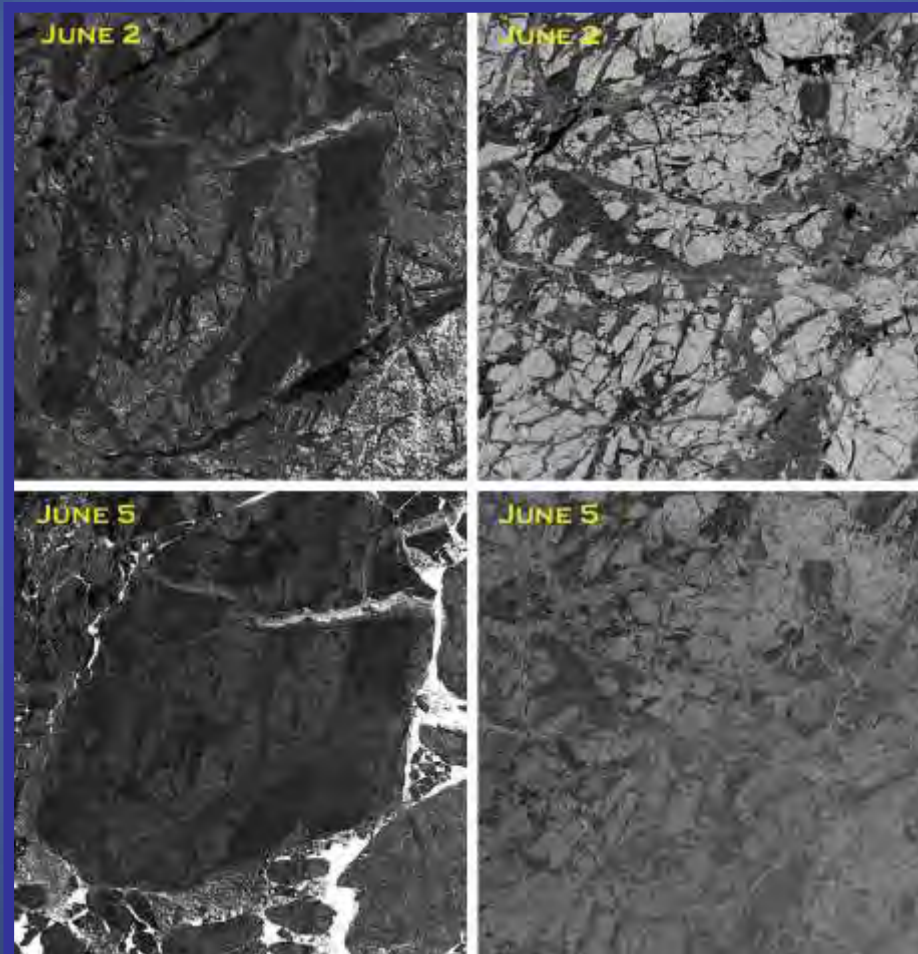
Airborne SAR sensor
ESAR (DLR)
19 March 2007, 12:26 UTC
spatial resolution 2 m

Spaceborne SAR sensor
ENVISAT ASAR WS (C-HH)
19 March 2007, 11:22 UTC
spatial resolution 150 m

[Dierking 2013]

Remote Sensing of Sea Ice

Influence of melting conditions (Beaufort Sea)

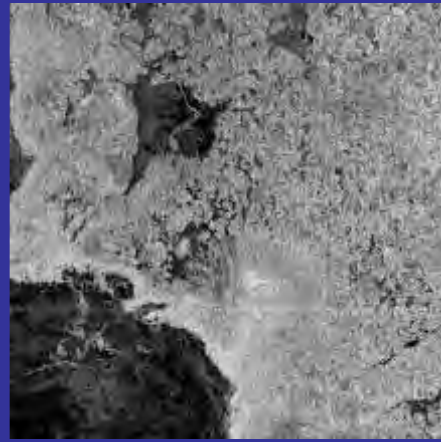


ENVISAT ASAR images
(C-HH, 90 km × 90 km,
 $19^\circ < \theta < 28^\circ$), © ESA

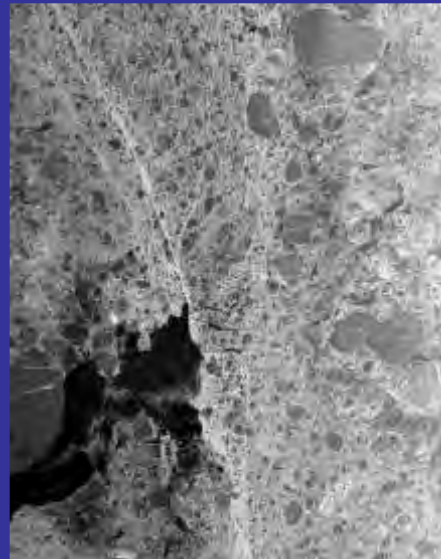
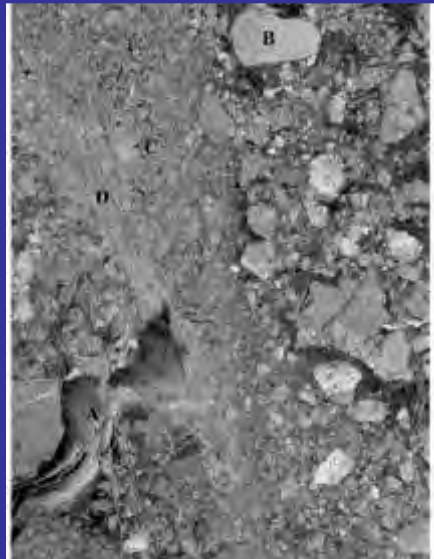
ENVISAT ASAR images
(C-HH, 90 km × 90 km,
 $35^\circ < \theta < 43^\circ$), © ESA

[Dierking 2013]

SAR Imaging of Sea Ice



SAR images (80 km × 80 km)
Arctic sea ice at 82°N 12°E
(19 September 1996, © ESA, CSA)
left: ERS (C Band, VV pol)
right: Radarsat (C Band, HH pol)



ERS SAR image (50 km × 65 km)
Arctic sea ice
(© ESA, NASDA)
left: ERS (C Band, VV pol)
right: JERS-1 (L Band, HH pol)

[Barale & Gade 2008]

Remote Sensing of Sea Ice

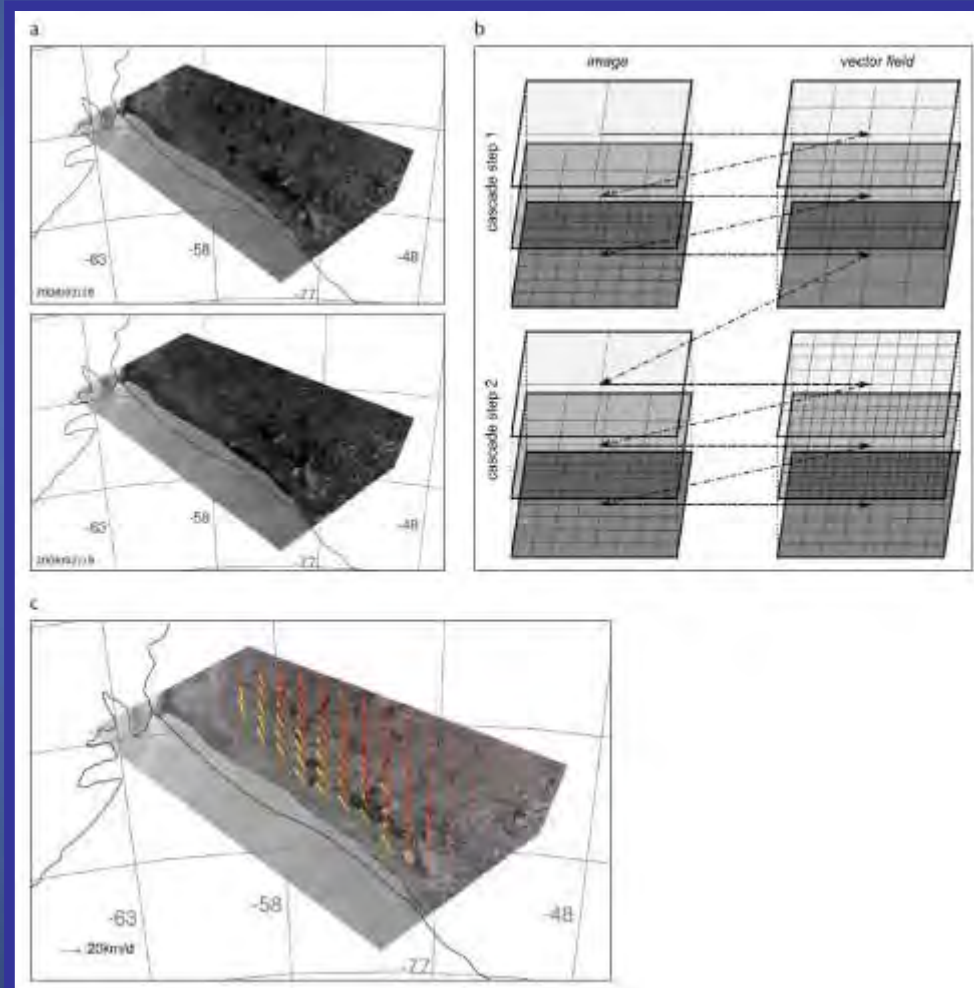
Ice-drift vectors derived from SAR imagery

ENVISAT ASAR images
(C-HH)
Ronne Polynya, Wedell Sea
© ESA

18 February 2008, 06:09 UTC

19 February 2008, 05:38 UTC

Drift vectors from
SAR image analysis (red)
and visual inspection (yellow)



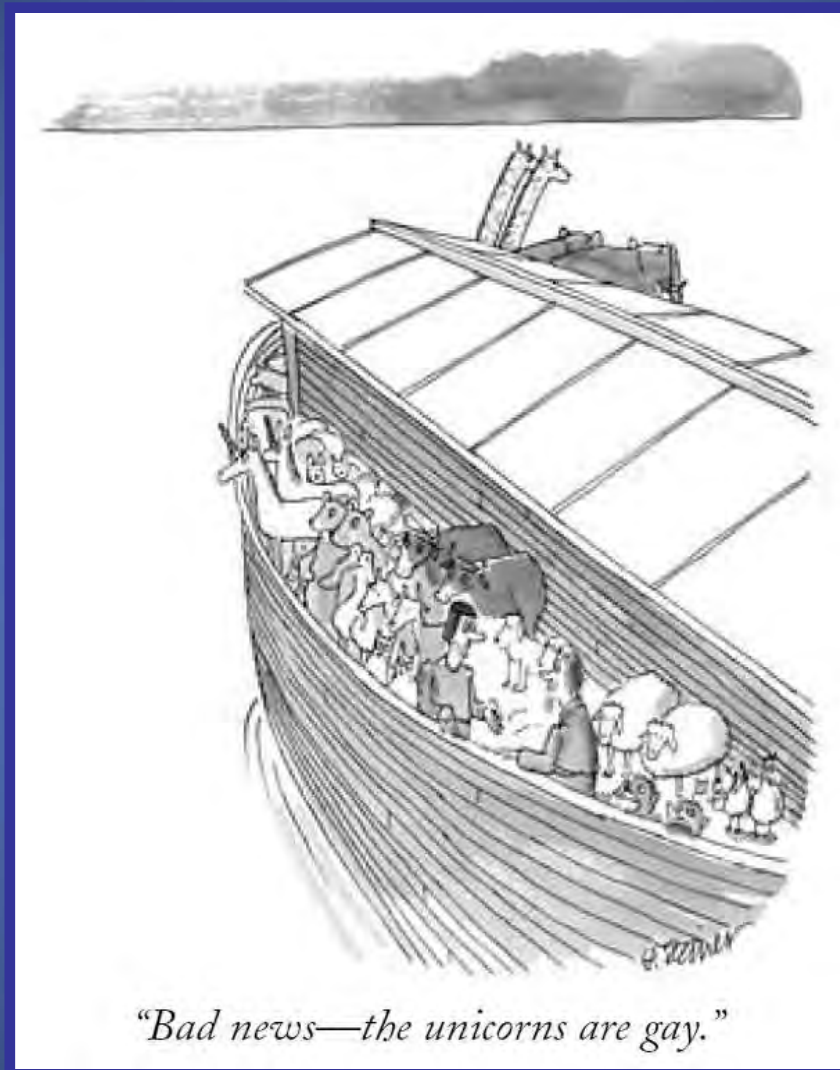
Drift analysis:
resolution pyramids
linked in a cascade

[Dierking 2013]



Sea Ice Take-Home Messages

Ice detection (icebergs)
Classification through multi-pol SAR
Ice drift



Ocean Features on SAR Imagery

Feature	Scale	Derived Measurement	Imaging Mechanism	Wind Speed Range [m s ⁻¹]	Characteristics and Considerations
Surface Waves	100 - 600 m wavelength	Wavelength Propagation direction Wave height	Tilt Hydrodynamic Velocity Bunching	3 – 40	Azimuth-traveling waves may be nonlinear without correction. Other limiting factors include wavelength, wave height and fetch.
Internal Waves	0.3 - 3 km wavelength	Wavelength Direction Amplitude Mixed layer depth	Convergence/Divergence Surfactants	2 – 10	Curvilinear packets with multiple waves, decreasing wavelength from front to back. Sensitive to wind conditions, wave crest orientation to platform.
Internal Tides	10 - 20 km	Wavelength Direction	Interaction of centimeter Waves/Currents/Surfactants	3 – 7	
Currents and Fronts	1 - 100 km	Location Shear Strain Velocity	Shear/Convergence Convergence Wind stress Surfactants	3 - 10 3 - 10 3 - 10 3 – 7	Sensitive to wind conditions. Often multiple mechanisms present simultaneously.
Eddies	1 - 200 km diameter	Location and source Diameter Velocity Shear Strain	Shear/Convergence Wind Stress Surfactants	3 - 10 3 - 10 3 – 7	Sensitive to wind conditions. Often multiple mechanisms present simultaneously.
Shallow Water Bathymetry	5 - 50 m depth	Location/change detection Current velocity Depth	Convergence	3 - 12	Sensitive to wind, current properties, depth.

[Jackson & Apel, 2004]

Air-Sea Interactions on SAR Imagery

Feature	Scale	Derived Measurement	Imaging Mechanism	Wind Speed Range [m s^{-1}]	Characteristics and Considerations
Surface Winds	> 1km grid	Wind speed Wind direction	Wind stress Indirectly via windrows, models, or sensors	3 – 25	For mesoscale, coastal variability. Requires good calibration.
Roll Vortices	1 - 5 km wavelength	Boundary Layer: Stratification	Wind stress	3 – 15	Long axis/crests parallel to wind direction.
Gravity Waves	2 - 10 km wavelength	Height Turbulence spectrum Drag coefficient	Wind stress	3 – 15	Long axis/crests perpendicular to wind direction, often associated with topography
Rain Cells	2 - 40 km diameter	Rain rate	Wind stress Rain damping	3 - 15	Appearance sensitive to frequency, rain rate, wind speed.

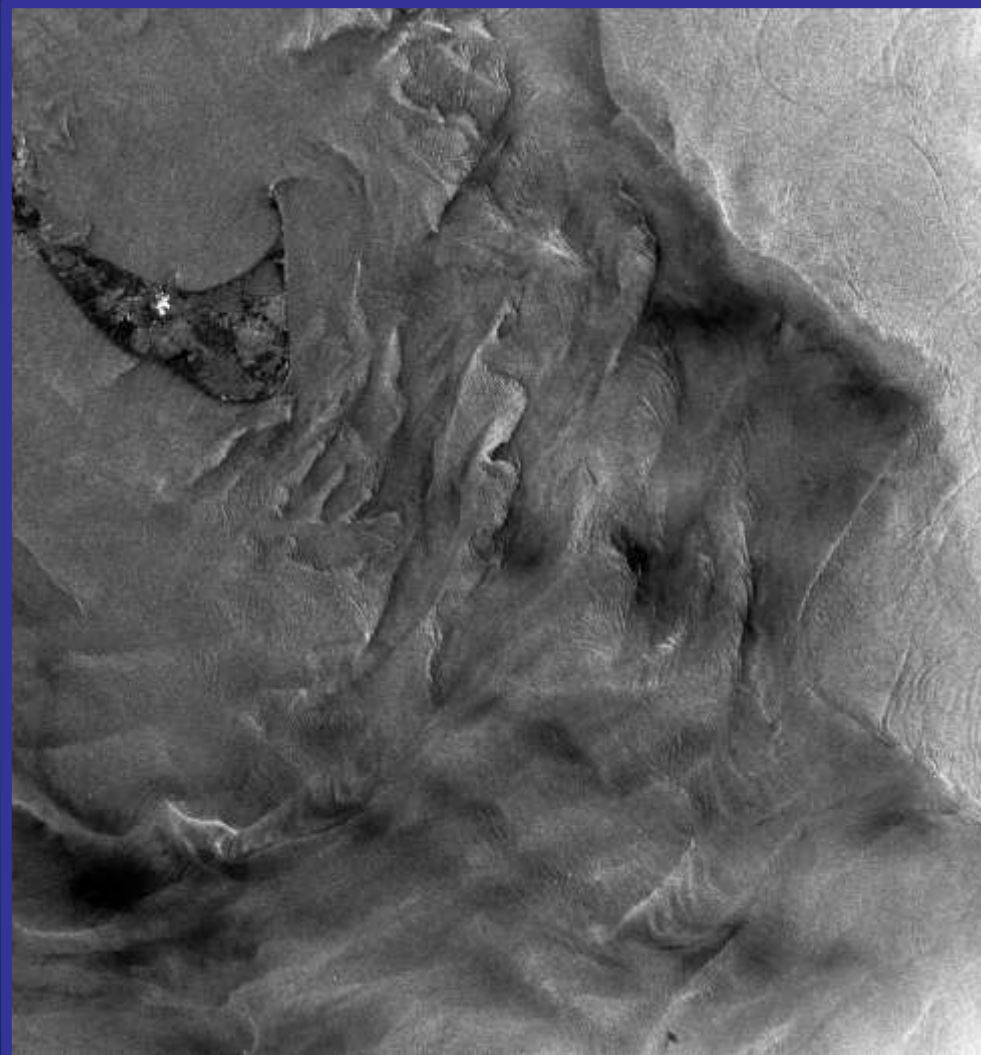
[Jackson & Apel, 2004]

Surface Films on SAR Imagery

Feature	Scale	Derived Measurement	Imaging Mechanism	Wind Speed Range [m s^{-1}]	Characteristics and Considerations
Biogenic Surfactants	> 100m ² area	Areal extent	Convergence	2 – 8	Both forms have signatures similar to low wind, cold thermal water masses, etc.
Mineral Oils	> 100m ² area	Areal extent	Seeps Ship discharge Run-off	3 – 15	Wind speed, combination of L- and C-/X-bands may enable discrimination of each form.

[Jackson & Apel, 2004]

Seasat SAR Image



What is shown here?

Seasat SAR Image (L-HH, 80 km × 75 km)
Nantucket Island
(27 August 1978, 12:34 UTC)



it's time for exercises...

it's time for exercises...